Sarabjeet Singh, Carl Q.Howard, Colin H.Hansen

An extensive review of vibration modelling of rolling element bearings with localised and extended defects

Journal of Sound and Vibration, 2015; 357:300-330

An extensive review of vibration modelling of rolling element bearings with localised and extended defects

Sarabjeet Singh[1,*], Carl Q. Howard, Colin H. Hansen

School of Mechanical Engineering, The University of Adelaide, Adelaide, South Australia 5005, Australia

Abstract

This paper presents a review of literature concerned with the vibration modelling of rolling element bearings that have localised and extended defects. An overview is provided of contact fatigue, which initiates subsurface and surface fatigue spalling, and subsequently leads to reducing the useful life of rolling element bearings. A review is described of the development of all analytical and finite element (FE) models available in the literature for predicting the vibration response of rolling element bearings with localised and extended defects. Low- and high-frequency vibration signals are generated at the entry and exit of the rolling elements into and out of a bearing defect, respectively. The development of this finding is described along with analytical models to approximate these vibration signals. Algorithms to estimate the size of bearing defects are reviewed and their limitations are discussed. A summary of the literature is presented followed by recommendations for future research.

Keywords:
rolling element bearing, localized defect, extended defect, vibration, spall, contact fatigue

1. Introduction

Rolling element bearings, also referred to as anti-friction bearings [1], are widely used in rotating machinery across various industries that include aerospace, construction, mining, steel, paper, textile, railways, and renewable energy [2]. The damage and failure of bearings contribute to machinery breakdown, consequently causing significant economic losses and even loss of human lives in certain situations; for example, when an aircraft engine fails or a train derails due to a bearing seizure. Undesirable vibrations in rolling element bearings can be caused by either faulty installation, poor maintenance and handling practices [3] or surface fatigue [4], which eventually leads to the formation of various types of defects [5], often referred to as spalls, within rolling element bearings. It is well-known that when a defective (spalled) component, either a rolling element, an outer raceway or inner raceway, within an operating bearing interacts with its corresponding mating components, either defective or non-defective, abrupt changes in the contact stresses occur [6]. These changes excite the bearing structure and encompassing structural components connected to the bearing, resulting in the generation of vibrations, and consequently acoustic signals, which can be monitored to detect the presence of a defect using appropriate condition-based (vibration and acoustic) diagnostic techniques [3, 6–18].

Since the early 1950s, numerous researchers have contributed, experimentally and analytically, with the ultimate objective to understand the vibration response of non-defective (ideal) [19–42] and defective rolling

*Corresponding Author. Tel.: +61 8 8362 5445; fax.: +61 8 8362 0793
Email addresses: sarabjeets@trackiq.com.au (Sarabjeet Singh), carl.howard@adelaide.edu.au (Carl Q. Howard), colin.hansen@adelaide.edu.au (Colin H. Hansen)
[1]Present Address: Trackside Intelligence Pty Ltd, 17–19 King William Street, Kent Town, South Australia 5067, Australia

element bearings [43–119]. Defects in rolling element bearings can be classified into three broad categories — localised [43–79], extended defects [68, 80], and distributed [81–119]. This paper presents a review of the first two.

This paper begins with a discussion of contact fatigue in rolling element bearings along with an overview of some typical bearing defects in Section 1.1. A review of the existing knowledge pertinent to the vibration response of rolling element bearings having localised defects obtained through experimental work [3, 76, 79, 120–124], a number of analytical [43–69], and FE models [70–79] is presented in Section 2. The vibration modelling of bearings having extended defects [68, 80] is discussed in Section 3. The characteristics of vibration signatures at the entry and exit of rolling elements into and out of a localised bearing defect [76, 77, 79, 120–124], respectively, along with the physics behind the generation of defect-related vibration impulses [76, 79] are discussed in Section 4. This is followed by a discussion on the estimation of an average size of a bearing defect [67, 76, 79, 124, 125] in Section 5. The existing knowledge is summarised in Section 6 followed by some future directions in Section 7.

1.1. Contact fatigue

Contact fatigue is a type of a surface defect or damage [126–128] that is inevitably related to the operational wear of rolling element bearings. It is generally characterised by spalling, pitting, or flaking off the metallic particles from the rolling surfaces of a bearing, namely outer raceway, inner raceway, and rolling elements [3–5, 129–132]. In the context of bearings, contact fatigue is also referred to as *rolling contact fatigue* because of the rolling and relative sliding movements of the rolling surfaces [130–132].

Loads acting between the rolling elements and raceways within a bearing develop only small areas of contact [133]; the geometry of the contact area and corresponding parameters, such as contact force, stiffness, and deformation, follow the classical Hertz theory of elasticity [134–136]. As a result, the elemental loading may only be moderate; however, the compressive stresses induced on the rolling surfaces of a bearing are extremely high — typically of the order of a few giga-pascals ($\approx$ 2–4 GPa) [132, 133].

It is considered that if a rolling element bearing in service is properly installed, aligned, loaded, lubricated, and kept free from contaminants, then the main mode of its failure is surface fatigue, which would result after an estimated number of rolling cycles (usually of the order of millions) [132, 133, 137, 138]. This (bearing) failure mode is also known as *fatigue spalling* or *pitting*, and is characterised by surface spalls or pits [3–5, 129–132].

1.1.1. Fatigue spalling

In a properly installed and lubricated bearing, the onset of micro-scale subsurface fatigue cracks commences below the highly stressed rolling surfaces. These cracks typically occur at micro-structural discontinuities, such as inclusions, inhomogeneity, or carbide clusters, as a result of micro-plastic deformation in the region of maximum stresses [139–149]. Due to the continuous and repetitive load (stress) cycles during the operation of a bearing, the micro-scale subsurface fatigue cracks continue to progress towards the surface, eventually causing the material to break loose or flake off, leading to the formation of macro-scale surface spalls or pits [3–5, 129–133]. Although spalls and pits are indiscriminately used in the literature to refer to the surface defects within rolling element bearings, Littman [4, 5] distinguished between the micro-scale subsurface and macro-scale surface originated fatigue cracks as spalls and pits, respectively [129].

Figure 1 shows a number of examples of fatigue spalling on various components of rolling element bearings: a few point spalls on the rollers are shown in Figure 1a, an area spall on the inner raceway is shown in Figure 1b, and area spalls of different characteristic shapes and sizes on the outer raceway are shown in Figures 1c and 1d.

In addition to the fatigue spalling, there are a number of other modes of bearing failure [151]. These failure modes include wear due to foreign material, smearing, etching–corrosion, brinelling, and burns from electric current discharge [3, 152]. Generally, these damages are caused by a variety of factors that include poor maintenance practices, mishandling, incorrect installation, misalignment, and inadequate lubrication. Often a bearing may commence to fail in one particular mode which then leads on to other failure modes [3]. These damages can cause premature surface fatigue, which eventually reduces the life of rolling element bearings.

(a) A few point spalls on the rolling elements.

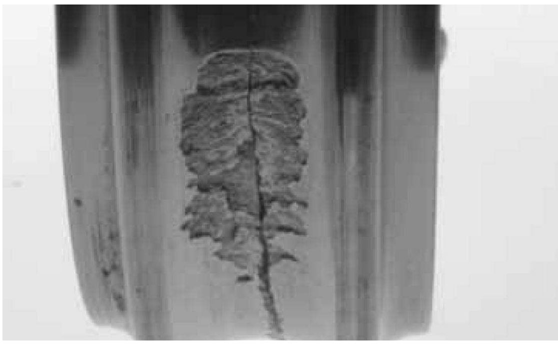

(b) An area spall on the inner raceway.

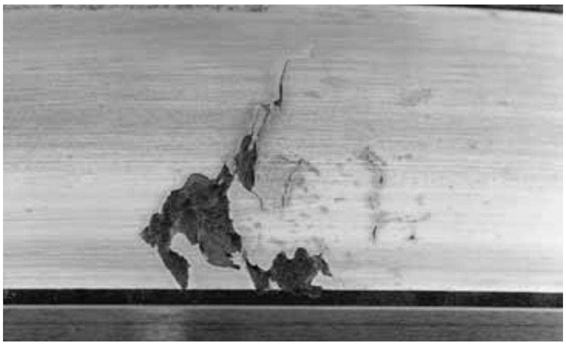

(c) An area spall on the outer raceway.

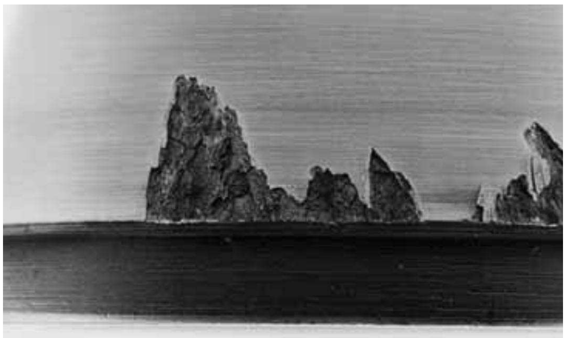

(d) An area spall on the outer raceway.

Figure 1: Fatigue spalls on various elements of rolling element bearings (courtesy: The Timken Company [150]; permissions to be obtained).

1.1.2. Rolling element bearing life

Understanding the cause for the onset of surface fatigue cracks is of significant interest not only to researchers, but also to bearing manufacturers as it has, historically, been considered to be a limiting factor for the useful life of rolling element bearings [153]. As a result, rolling contact fatigue mechanisms in bearings leading to their life estimation have been investigated by several researchers [154–191]. In the literature, these models are divided into two categories [132] — probabilistic engineering models [154–179] and deterministic research models [180–191]. In general, the engineering models are empirical in nature; they attempt to predict fatigue lives using solutions of the elastic stress field with the scatter in life being incorporated directly using the Weibull probability distribution function [192–194]. In contrast, the research models are mechanistic in nature; they assume an initial crack (either surface or subsurface) of a given length and orientation, and use fracture mechanics [126–128] to predict the shape of the spall and fatigue life of the contact.

The Lundberg–Palmgren model

In 1924, Palmgren [137] published a paper outlining his approach to bearing life prediction and an empirical formula based upon the concept of an L_{10} life, or the time that 90% of a bearing population would equal or exceed without a fatigue failure. Later on, in 1947, Palmgren along with Lundberg, incorporated his previous work [137] with the work of Weibull [192] to present the pioneering mathematical formulation for calculating the fatigue life of rolling element bearings [154, 155]. Their theory is commonly known as the *Lundberg–Palmgren theory*. It states that for bearing rings subjected to N cycles of repeated (stress) loading, the probability of survival S is given by

$$\ln \frac{1}{S} = A \frac{N^e \tau_0^c V}{z_0^h} \tag{1}$$

where, τ_0 is the maximum orthogonal shear stress in the contact, z_0 is the corresponding depth at which this stress occurs, and V is the stressed volume of material. The parameters A, c, and h are material characteristics that are determined experimentally, and the parameter e is the Weibull slope for the experimental life data plotted on a Weibull probability paper.

Since the development of the Lundberg–Palmgren theory, significant advances have been made in bearing material quality, fracture mechanics, and in the understanding of the role of lubrication through the development of elasto-hydrodynamic lubrication (EHL) theory [131, 195–201], in order to increase the fatigue life of rolling element bearings. The recognition of the limitations of the original Lundberg–Palmgren theory [154, 155] has led to the development of better and improved bearing fatigue life prediction models. The current ISO (International Organization for Standardization) [170], ANSI (American National Standards Institute, Inc., and ABMA (American Bearing Manufacturers Association, Inc.) [202, 203] standards for rolling bearing life are based on modifications of the Lundberg–Palmgren equation [154, 155]; the modifications account for the significant changes in relatively recent material quality, reliability, and operating conditions. Excellent reviews of the bearing life models can be found in references [132, 171, 177, 204].

The following sections present a review of all analytical [43–69] and FE models [70–79] available in the literature for predicting the vibration response of defective rolling element bearings having localised and extended defects.

2. Localised defects

Localised defects, one of the two main classes of bearing defects, include cracks, pits, and spalls on various components of a rolling element bearing. The components within a bearing refer to its rolling surfaces — outer raceway, inner raceway, and rolling elements. The localised defects are an ultimate failure mode of a correctly installed and lubricated bearing during its normal operational use. A few examples of surface fatigue spall, localised defects, are shown in Figure 1.

In order to present a systematic review of analytical and FE models that predict the vibration response of rolling element bearings that have localised defects, the models are classified into four broad categories as follows:

1. Periodic impulse-train models [43–46]
2. Quasi-periodic impulse-train models [47–52]
3. Nonlinear multi-body dynamic models [53–69]
4. FE models [70–79]

2.1. Periodic impulse-train models

A *periodic* impulse-train model refers to an analytical model that simulates the generation of defect-induced impulses at a constant period. Such a model does not include the physical parameters of a bearing, such as masses of bearing components, nor attempts to simulate the deformation at the rolling element-to-raceway contact interfaces that is governed by the Hertzian contact theory of elasticity [134–136]. For the case of a stationary outer raceway defect, the impulses are equally spaced, and their characteristics, such as shape, amplitude, and width, are similar to each other. On the contrary, for a rotating inner raceway defect and a rolling element defect, the impulses are generally modulated as per the static load distribution within a rolling element bearing; that is, the amplitude of the defect-induced impulses varies as the inner raceway and rolling element defects rotate in and out of the bearing load zone [2, 205–208].

The first model for simulating the vibration response of a localised single point defect on the inner race of a rolling element (ball) bearing, under a constant radial load, was developed by McFadden *et al.* [43] in

1984. The forces produced by the point defect were modelled as an infinite series of periodic force impulses of equal amplitude using the Dirac delta function [209, pages 9–10] with a period T as

$$I(t) = \sum_{i=-\infty}^{\infty} \delta(t - iT) \tag{2}$$

where, $I(t)$ is the impulse force, δ is the Dirac delta function, t is the time vector, and T is time period of the defect-related impulses. The resonance characteristic in the Fourier domain [210] was sampled at the regular interval of $1/T$. Based on the assumption that the amplitude of the impulse produced by a defect is directly proportional to the load on a rolling element when it strikes a defect, the amplitude of the impulses was multiplied by the actual load on the rolling elements, estimated using the well-known Stribeck equation [205].

McFadden *et al*. further extended their defect-induced impulse-train model [43] to incorporate two point defects located on the inner race of a ball bearing [44]. The effects of two point defects were simulated by treating the defects as the sum of a number of localised defects at different angular locations around the inner raceway. Both models [43, 44] incorporated the effects of bearing geometry, shaft rotational speed, bearing load distribution, and the exponential decay of vibration. Satisfactory validation of both models was reported on the basis of agreement of the predicted vibration (line) spectra with experimental results after conducting a standard envelope analysis [211, 212]. While McFadden *et al*. did not predict the absolute amplitude of the defect-related frequency components, fundamental and harmonics, in their first model [43], the predicted amplitudes in their second model [44] were corrected based on their experimental results. They found that the demodulated (also known as envelope) vibration spectrum was composed of groups of discrete frequency components, separated by the shaft rotational frequency f_s, while the spacing between the successive groups was the inner raceway defect frequency f_{bpi} (also known as ball pass frequency inner raceway — BPFI; refer to Appendix A for the definition of BPFI and other defect frequencies associated with rolling element bearings). The aforementioned models provided some early insights into the demodulated vibration spectrum of a rolling element bearing obtained through accelerometer measurements in practice, and partially helped explain the defect-related frequency components, fundamental, sidebands, and associated harmonics, in a measured vibration spectrum. The models developed by McFadden *et al.* [43, 44] are often referred to as *classical* or *traditional* models in the literature.

Su *et al.* [45] extended the models developed by McFadden *et al*. [43, 44] to predict the vibration frequencies produced by a single point defect and multiple (two) point defects within a rolling element bearing subjected to various types of loads. They proposed periodicities that include fundamental defect frequencies, sidebands and associated harmonics, for the outer raceway, inner raceway, and rolling element defects due to various load conditions. These load conditions include shaft unbalance and roller errors, in addition to the case of stationary loading along the circumference of the inner race as considered by McFadden *et al.* [43, 44]. Su *et al.* [45] reported that for a fixed outer raceway defect, the vibration signature of a bearing has periodicities at $1/f_s$ and $1/f_c$ due to shaft unbalance and roller errors, respectively, where, f_s is the shaft rotational frequency, and f_c is the cage rotational frequency. However, for an inner raceway defect, the vibration response of a bearing has no periodicity due to shaft unbalance, but a periodicity of $1/(f_s - f_c)$ due to roller errors. The comparison of the predicted defect-related frequencies and sidebands with the experimental results showed good agreement. The effect of the loading distributions due to shaft unbalance and roller errors provided further explanation of the spectral content of the demodulated vibration spectrum of a bearing for cases in addition to the cases considered by McFadden *et al.* [43, 44].

In the late 1990s, Tandon *et al.* [46] proposed an analytical model for predicting the vibration frequencies, fundamental and harmonics, of a rolling element bearing along with the amplitudes of the frequency components, caused by a localised single point defect on the outer raceway, inner raceway, and one of the rolling elements, under radial and axial loads. Similar to previous models [43–45], Tandon *et al.* [46] also modelled the vibration response using periodic impulse-trains; however, they considered three different types of typical pulse shapes of finite width — rectangular, triangular, and half-sine. The results showed that for an outer raceway defect, a vibration response is generated at the outer raceway defect frequency f_{bpo} and its multiples. For an inner raceway defect, a response is generated at the inner raceway defect frequency

f_{bpi} in the absence of a radial load; however, in its presence, a response is also generated at equi-spaced sidebands at the shaft rotational frequency f_s in addition to the inner raceway defect frequency f_{bpi}. Tandon *et al.* [46] also reported that the vibration amplitude due to the outer raceway defect was higher compared to that of the inner raceway defect, and the amplitudes of the vibration frequencies and their harmonics were affected by the different pulse shapes. Although a fair agreement between the predicted and experimental results was claimed, the comparison was only illustrated for the defect on the inner raceway of a bearing. Tandon *et al.* [46] also mentioned that the amplitudes of the predicted frequency components were normalised (or corrected) for the comparison with the experimental results; however, the normalisation factor was not discussed. The problem of amplitude mismatch has also been highlighted by several other authors [56, 57, 62–64] who, later on, developed nonlinear multi-body dynamic models. These models will be discussed in Section 2.3.

2.2. Quasi-periodic impulse-train models

A *quasi-periodic* or an *aperiodic* impulse-train model refers to an analytical model that includes some random fluctuations due to the slip between the rolling elements and the raceways within a bearing [48, 49]. These quasi-periodic impulse-train models are also referred to as *stochastic* models.

The periodic impulse-train models [43–46] were based on the consideration of equi-spaced generation of force impulses as the rotating components within a bearing repetitively pass over a defect. However, based on the observations of the experimental results of a ball bearing having an inner raceway defect, Brie [47] suggested that the defect-induced excitation cannot be considered as periodic, but quasi-periodic in nature. As the earlier models [43, 44] could not explain some frequency variations, Brie modelled the response of a bearing using a single-degree-of-freedom (DOF) lumped mass-spring-damper system. A slight variation was introduced to the modelled defect-induced impulse-train, although the cause and amount of the variation were not mentioned.

Ho *et al.* [48] and Randall *et al.* [49] explained that the slippage of the rolling elements causes slight random variation in the spacing between two consecutive defect-related impulses observed in practice. They explained that the random variations occur due to the slip associated with the motion of the rolling elements within a bearing — the contact angle between rolling elements and raceways varies with the position of each rolling element. As a result, each rolling element has a different effective rolling diameter and tries to roll at different speeds. However, the cage limits the deviation of the rolling elements causing some slip and consequently variations between the time intervals associated with the defect-related impulses. These slight random variations lead to smearing in the frequency spectrum of defect-related harmonics at higher frequencies; that is, defect-related frequencies appear as discrete harmonics of negligible amplitude in the low frequency region, but smeared in the high-frequency region where their amplitude is amplified by correspondence with the structural resonance frequencies of a bearing [17].

In order to address the deficiencies in prior models [43–46], Ho *et al.* [48] also modelled the localised defect-induced vibration signals as a series of impulse responses of a 1-DOF system. However, they introduced random variations in the time between the impulses so as to gain a close resemblance to measured vibration signals. The results showed that the incorporation of the fluctuations in the modelled signals provided a realistic update to the traditional models proposed by McFadden *et al.* [43, 44]. The work presented by Ho *et al.* [48] was primarily focused at investigating bearing diagnostic techniques, such as self-adaptive noise cancellation [213] and squared envelope analysis rather than investigating the vibration characteristics.

Adopting the model of Ho *et al.* [48], a few more authors have also incorporated the slippage-related random fluctuations in their proposed defect-induced impulse-train models [49–51]. The force impulses in these models [49–51] were simulated using a 1-DOF system [49] and the Dirac delta function [50, 51]. The authors of the models [49–51] used the theory of cyclostationarity [214–218], and characterised the bearing signals as quasi-cyclostationary; that is, their statistics are quasi-periodic [49] as indicated by Brie [47]. The emphasis of the stochastic models presented in references [48–51] was focused on the diagnostics of defective rolling element bearings using cyclic spectral density analysis [17, 216, 217].

Unlike the technique used by previous researchers [43–51] for generating the defect-induced impulse-trains, Behzad *et al.* [52] applied the concept of rough elastic contact between the surfaces of a rolling element bearing. Rough elastic contact mechanics has been exploited by several researchers to analytically model rough surfaces [136, 219–228] and explain the source of high-frequency vibrations in rolling contacts with attention focused on wheel–rail contact [229–239] and rolling element bearings [240, 241]. Behzad *et al.* [52] presented a stochastic model for estimating the vibration response of defective rolling element bearings. They considered two measures of roughness to represent non-defective and defective surface areas using the Gaussian probability distribution [242, pages 59–66]; the localised outer raceway defect had a rougher surface than the non-defective bearing surfaces. Assuming the applicability of the Hertz theory of elasticity [134–136], variations in the contact forces between the rolling elements and raceways contact interfaces were estimated on the basis of the roughness-related profiles of the rolling surfaces [52]. As the defective surface was modelled as rougher compared to the non-defective surfaces, high magnitudes of contact forces, and consequently vibrations, were generated at the interaction of the rolling elements and the summits of the asperities at the localised defective area, compared to rolling elements and non-defective areas. Behzad *et al.* [52] showed that the predicted vibration response agreed well with the experimental measurements. They also reported that the performance of their stochastic model was better than the traditional periodic impulse-train models [43, 44]; however, the performance was not compared with previous stochastic models [48–51]. It is important to note that the randomness or stochasticity in the model proposed in reference [52] is due to the roughness profile of the surfaces, and not due to the slippage of the rolling elements [48, 49]. Therefore, their model effectively generates periodic force impulses.

The valuable insights into the vibration spectra of defective rolling element bearings, gained through the impulse-train models [43–52], provided motivation for subsequent researchers to incorporate various components of a bearing and bearing–housing in rotor–bearing systems in their models, which led to the development of nonlinear, multi-body dynamic models [53–69], and are reviewed in the following section.

2.3. Nonlinear multi-body dynamic models

The nonlinear multi-body dynamic analytical models of rolling element bearings and associated systems are lumped parameter models. In the context of mechanical systems, a *lumped parameter* model simulates various elements or components of a system as simplified rigid masses connected by a series of springs (to model linear or nonlinear contact interfaces) and dampers (to account for energy losses). The nonlinear multi-body dynamic models for predicting the vibration response of a bearing, bearing–pedestal (housing), and rotor–bearing systems, due to the presence of localised bearing defects [53–69] generally consider the outer and inner rings as lumped (rigid) masses and the rolling elements-to-raceways contact interfaces as nonlinear springs. The localised defects not only include point spalls [53, 56, 57, 59, 61, 62] (as considered for the impulse-train models [43–51]), but also circular spalls [60, 64], elliptical spalls (as ellipsoids for ball bearings) [66] as a function of the Hertzian contact deformation [134–136], and line (rectangular) spalls [54, 55, 58, 63, 65, 67–69] as a function of width and depth.

The common feature of all models in references [53–69], except the models in references [66, 67], is that they neglect the bending (flexural) deformation of the outer and inner rings, and rolling elements. However, all models consider the localised nonlinear Hertzian contact deformation at the rolling element-to-raceway contact interfaces. In order to simplify the analysis, the majority of the multi-body models use the following assumptions:

1. The outer and inner rings are rigidly connected to the housing [53–65, 68, 69] and shaft [53–69], respectively.
2. The rolling elements are excluded or considered massless [53–56, 58–60, 62–64, 67, 68].
3. The inertial and centrifugal effects of the rolling elements are ignored [53–64, 66–68].
4. The slippage of the rolling elements [49] is ignored [53–57, 59–65, 67]; thus, eventually resulting in the generation of periodic defect-induced impulses.
5. The EHL fluid film [131, 195–201] in rolling contacts is ignored [56, 58–64, 66, 67].
6. The stiffness of a bearing is considered to be linear [54–56, 59, 60, 62–64, 66–68].

Prior to investigating the vibration response of rolling element bearings (and associated bearing–pedestal and rotor–bearing systems) due to the presence of defects, the research was primarily focused on understanding the characteristics of the vibration response of non-defective bearings [19–42]. The first systematic investigations were conducted by Perret [19–22] and Meldau [23–26] in the early 1950s. They concluded that rolling element bearings generate cyclic vibrations even in the absence of manufacturing or geometrical imperfections; such vibrations are commonly referred to as *variable compliance vibrations*, which were later described by Sunnersj [92, 93]. A significant number of experimental and analytical studies on the characteristics of vibrations caused by the geometrical imperfections in rolling element bearings, such as surface roughness, waviness, misaligned raceways, off-sized rolling elements, and out-of-round components, were carried out by Svenska Kullagerfabriken AB (SKF) Industries, Inc. [243], and 17 bi-monthly reports were issued. A few special reports can be found in references [81–86], and the summary of the overall work in reference [88]. Later, several researchers reported on the development of analytical models to predict the vibration response of rolling element bearings due to various distributed defects with attention focused on the waviness of raceways and rolling elements [87, 89–119]. However, from the review of the literature conducted during the course of this paper, it appears that *the first nonlinear multi-body dynamic model* for predicting the vibration response of a rolling element bearing (in a bearing–pedestal system), due to a localised (point) defect, was reported in 2002 by Feng *et al.* [53]. Their model was an extension to the model developed by Fukata *et al.* [40] that describes the vibration response of an ideal (non-defective) ball bearing. Fukata *et al.* [40] modelled a rotor–bearing system as a simplified 2-DOF system; while the outer ring was modelled to be stationary, the inner ring was assumed to translationally move in the radial plane (of the model) with two degrees of freedom (global Cartesian x- and y-directions).

In order to present a review of the nonlinear multi-body dynamic analytical models [53–69] for predicting the vibration response of rolling element bearings having localised defects, the models are segregated into three categories based on the characteristic shape of the defects being considered:

1. Point spall [53, 56, 57, 59, 61, 62]
2. Circular and elliptical spall [60, 64, 66]
3. Line (rectangular) spall [54, 55, 58, 63, 65, 67–69]

2.3.1. Point spall

Building on the 2-DOF model of Fukata *et al.* [40], Feng *et al.* [53] presented a 4-DOF model corresponding to the two translational degrees of freedom, in the radial plane, each for the two lumped masses: the rotor and pedestal masses. No other component was included in the model except the outer ring, which was assumed to be stationary and rigidly connected to the pedestal. As the primary aim of the model [53] was to demonstrate the working capability of the in-house transient analysis software [244] to simulate the vibration signals due to localised bearing defects, the characteristic dimensions and parameters of the rotor–bearing system model were fictitiously chosen. The 4-DOF model was solved using the fourth-order Runge-Kutta integration scheme [245, Chapter 5], which was incorporated in the developed software [244]. The results of the numerical simulations were not compared with any kind of experimental results, but were simply validated by comparing the values of the defect-related frequency components, f_{bpo} and f_{bpi} for outer and inner raceway defects, respectively (obtained from an envelope analysis [211, 212] of the modelled signals), using the existing knowledge on the basic bearing kinematic defect frequencies (as described in Appendix A). Despite being the first multi-body analytical model for predicting the vibration response of a rolling element bearing having a localised point spall, the model by Feng *et al.* [53] has been overlooked by many researchers that developed their own models. This is probably because it was not published in a journal, but presented at a conference. However, the 4-DOF model of Feng *et al.* [53] was extended by Sawalhi *et al.* [58, 80] which is described later in Section 2.3.3.

In 2006, Choudhury *et al.* [56] proposed a 3-DOF lumped mass-spring-damper model for predicting the vibration response due to a localised point spall on various elements of a rolling element bearing in a rotor–bearing system. Similar to the assumptions considered in the models developed earlier [53–55], Choudhury *et al.* [56] also considered the outer and inner rings as rigidly connected to the housing and shaft, respectively. The rolling elements were excluded from the model, and on the basis of the findings reported in references [246, 247], the stiffness of the bearing was considered to be linear. The defect-related force impulses were generated as a rectangular-shaped periodic impulse-train without including the slippage of the rolling elements [49]. For the outer raceway defect, it was shown that the amplitude of the vibration (velocity) increased with increasing harmonic order, and for the inner raceway defect, the sidebands (f_s and $f_{\mathrm{bpi}} \pm f_s$) were asymmetrically distributed about the defect frequency. The modelling results (vibration line spectra) for only the inner raceway and rolling element defects were compared with the experimental results. Similar to the findings reported in previous references [46, 54, 55], Choudhury *et al.* [56] also reported that the amplitude of the frequency components for the outer raceway defect was much higher than that for the inner raceway and rolling element defects. Although a fair agreement between the predicted and experimentally measured defect-related frequency components was shown, their amplitudes did not match well with each other. However, despite their earlier findings reported in reference [46] (reviewed in Section 2.1) related to the effect of different pulse shapes (rectangular, triangular, and half-sine) on the amplitudes of defect-related frequencies, Choudhury *et al.* [56] restricted the usage of the pulse shape to rectangular in their proposed multi-body model. The significant mismatch between the amplitude of the frequency components could be due to the (assumed) rectangular shape of the modelled impulses and unknown characteristics of the actual defect-induced impulses. They also mentioned that the predicted results were normalised for the comparison purposes [56]; however, did not provide the normalisation factor, which was the same limitation found in their previous work [46].

In 2007, Sassi *et al.* [57] presented a numerical model to predict the vibration response of a deep-groove ball bearing having a localised point spall on the outer and inner raceways, and one of the rolling elements within the bearing. Although the majority of the simplifications considered during the modelling were similar to earlier models [53–56], Sassi *et al.* [57] included the rolling elements (balls) as rigid bodies (lumped point masses), and this was excluded in previous work [53–56]. The defect-related impulses were mathematically modelled as periodic impact forces, and the empirical expression for estimating the impact force was taken from reference [248]. The equations of motion for the coupled 3-DOF system representing the rotor–bearing system [57] were solved using Simulink® [249], and compiled as a toolbox, BEAT (BEAring Toolbox) in the MATLAB® software [250]. Time and frequency domain analyses were conducted on the simulated data, and the predicted results from the model were compared with the experimental results obtained from the bearing data centre at Case Western Reserve University (CWRU) [251]. Similar to the problem encountered by previous researchers [44, 46, 56], Sassi *et al.* [57] also reported the amplitude mismatch between the predicted and experimental defect-related frequency components; fundamental, sidebands, and harmonics. They mentioned that the amplitude of the predicted frequencies was corrected in order to simply match them with the corresponding experimental results; however, similar to the approach taken by previous researchers [46, 56], the amplitude-correction factor was not discussed.

For a coupled shaft–bearing system, Arslan *et al.* [61] proposed a 3-DOF lumped parameter model. In contrast to the previous models in references [53–59], which presented the vibration response of either the bearing or housing, the model in reference [61] presented displacement of the rolling elements (balls) within the bearing. Although the point mass of rolling elements was included in the model, their inertial and centrifugal effects were ignored as was done in reference [57]. Arslan *et al.* [61] neither reported on the conduct of the experimental work, nor carried out a comparison of their modelling results with the results from the literature.

In 2009, Rafsanjani *et al.* [62] presented a 2-DOF multi-body model to study the stability of a rotor–bearing system having a localised point spall on various elements of a ball bearing. The model was based on the work of Sunnersjö [93] who also presented a 2-DOF model to demonstrate a method for the estimation of the variable compliance vibration frequencies [88]. The two translational degrees of freedom were related to the displacement of the inner ring in the radial plane (global Cartesian x- and y-directions). Similar to the models in references [54–58], the outer and inner rings were rigidly connected to the housing and shaft, respectively, the nonlinear Hertzian contact deformation [134–136] was considered at the rolling element-to-raceway contact interfaces, the inertial and centrifugal effects of the rolling elements were ignored, and the stiffness of the bearing was considered to be linear [246, 247]. The effect of the localised defects was modelled as periodic impulses ignoring the slippage [49] of the rolling elements. Rafsanjani *et al.* [62] did not conduct any experimental work; however, in a similar way to reference [57], they used the experimental data available at the bearing data centre at CWRU [251] for the comparison of their modelled results. Similar to the problem encountered by previous researchers [44, 46, 56, 57], a substantial amplitude mismatch between the predicted and experimental results for the defect-related frequency components was also reported by Rafsanjani *et al.* [62].

2.3.2. Circular and elliptical spalls

Defect-induced periodic impulse-trains were generated using the Dirac delta function [209, pages 9–10] in the earlier models in references [43–46] to primarily understand the vibration-related spectral content of rolling element bearings that have a localised defect. In 2008, Ashtekar *et al.* [60] presented a new technique to model the localised defects on the raceways of deep-groove and angular contact ball bearings, and studied their effect on the bearing dynamics. They simulated the defect-related impulses by developing a mathematical expression to modify the deflection exponent n in the well-known Hertzian contact force-deflection (also referred to as load-displacement) relationship [134–136], $F = K\delta^n$, where F is the force, K is the contact stiffness, δ is the deflection, and n is the exponent, which is $3/2$ for point, circular, and elliptical contacts in ball bearings, and $10/9$ for line and rectangular contacts in roller bearings. The expression presented in reference [60] is a function of the load, ellipticity ratio, and the dimensions of the circular defect (diameter and height). It was used to estimate the modified contact forces at the interaction of the rolling elements and the defect in order to periodically simulate the force impulses. Ashtekar *et al.* [60] did not present a comparison of the modelling results with any experimental measurements.

Based on the earlier models in references [40, 62], Patil *et al.* [64] reported on the development of a 2-DOF lumped parameter model in order to study the effect of the size of localised raceway defects on the vibration response of a deep-groove ball bearing. The shape of the defects was modelled as a half-sine wave, and three defect sizes were considered (diameters as 0.5 mm, 1 mm and 1.5 mm). The modelling results [64] showed that the amplitude of the vibration spectra increased with increasing defect size for both inner and outer raceway defects. The experimental results were only shown for the outer raceway defect. The comparison of the modelled and experimental results showed that neither the outer raceway defect frequency component f_{bpo} and associated harmonics nor their amplitudes matched with each other. While the percentage error of approximately 6% was reported between the modelled and measured frequency components, the percentage error between their amplitudes, shown as an acceleration power spectrum (linear), was approximately 60,000%. The mismatch between the modelled and measured frequencies could be due to the neglect of slippage [49] of the rolling elements, whereas the amplitude mismatch problem has also been reported by others [44, 46, 56, 57, 62, 63].

Based on the previous 2-DOF models reported in references [40, 62, 64], Tadina *et al.* [66] proposed a numerical model to simulate the vibration signatures of a ball bearing having localised defects during run-up. In contrast to all the multi-body models [53–65], Tadina *et al.* [66] modelled the outer ring as deformable, using finite elements (two-noded locking-free shear, curved beam elements [252]). Although it was mentioned that the slippage or sliding between the components of the bearing was given by a prescribed function within the model, from the set of equations provided in the text, the slippage-related function could not be found. The localised defects on the raceways were modelled as impressed ellipsoids, which are formed due to the application of a radial load between the raceways and rolling elements of a bearing. On the contrary, the defect on a ball was modelled as a flattened region. An envelope analysis [211, 212] was conducted on the simulated results to highlight the defect-related frequencies. Tadina *et al.* [66] neither conducted the experimental work to measure the vibration response of defective rolling element bearings nor compared their results with the literature.

2.3.3. Line (rectangular) spall

With the objective of acting as an interface element between the rotor and supporting structure, Sopanen *et al.* [54, 55] developed a nonlinear multi-body dynamic model of a deep-groove ball bearing. Their 6-DOF model considered the outer and inner rings of the bearing as rigidly connected to the housing and shaft, respectively, the nonlinear Hertzian contact deformation [134–136] at the rolling elements-to-raceway contact interfaces, and the EHL fluid film in the rolling contacts [131, 195–201]. In addition to modelling the localised line spalls on the outer and inner raceways, surface waviness (one of the distributed defects [81–119]) of the raceways was also considered. The model was solved using a commercial multi-body software package, MSC Adams [253]. While Sopanen *et al.* [54, 55] did not conduct any experimental work, they compared their modelling results with those of similar studies available in the literature. For example, for the localised raceway defects, the predicted results were compared with the results in reference [46], and for the waviness, the modelling results were compared with the results reported in references [97, 98, 103, 107]. Sopanen *et al.* [54, 55] observed that the diametral clearance has a significant effect on the vibration response of the modelled rotor–bearing system, and the amplitude of the defect-related frequency components for similar defects was higher for the outer raceway defect in comparison to the inner raceway defect. The former observation was also reported by Tiwari *et al.* [105, 106], and the latter by Tandon *et al.* [46]. Sopanen *et al.* [54, 55] ignored the slippage of the rolling elements (balls) [49] and neglected the centrifugal forces acting on them, although it was shown that the modelled defect-related frequencies agree well with the earlier results published in the literature [46, 97, 98, 103, 105–107].

In 2008, Sawalhi *et al.* [58] extended the work of Fukata *et al.* [40] and Feng *et al.* [53], and developed an analytical model to simulate the vibration response of a defective ball bearing in a gearbox having localised line spalls. In contrast to the 2- and 4-DOF models presented in references [40] and [53], respectively, the model developed by Sawalhi *et al.* [58] comprised 5-DOF (translations in global Cartesian x- and y-directions) — 2-DOF for the inner ring, 2-DOF for the pedestal, and one for measuring the high-frequency response of the pedestal. Unlike the multi-body models reviewed so far [53–57], the lumped mass-spring-damper bearing–pedestal model by Sawalhi *et al.* [58] incorporated the slippage of the rolling elements [49] as a percentage variation (1% to 2%) of the defect-related frequencies in order to improve the match with measured vibration signals. Localised line spalls on the outer raceway, inner raceway, and a rolling element of a bearing were modelled by developing mathematical expressions based on the assumed path (trajectory) of the rolling elements as they traverse through the defect. Although the shape of the defects was modelled as rectangular, the definition of the path was based on the hypothesis that the rolling elements gradually enter into and exit out of the defect. However, inertial and centrifugal effects of the rolling elements were ignored. In the model by Sawalhi *et al.* [58], a set of relevant ordinary differential equations of motion for the coupled bearing–pedestal system to simulate its vibration response was solved using Simulink® [249]. A unique feature of the model presented by Sawalhi *et al.* [58] is that the pedestal was modelled using an additional mass-spring-damper system, referred to as a *resonance-changer,* attached to it. With the aim to simulate a typical high-frequency resonant response of a bearing, the values of the mass (1 kg) and the stiffness of the resonance-changer (8.89 N/m) were selected to excite the bearing at 15 kHz (with a damping of 5%). As the resonant mode of the bearing structure was deliberately chosen to be 15 kHz, the magnitude of the simulated vibration response due to the introduction of localised defects was higher around that frequency compared to the response of a non-defective bearing. Due to the mismatch between the modelled and actual resonant modes of the structure, different frequency bands were used to optimally demodulate the simulated and experimentally measured vibration signals using spectral kurtosis [12, 13] and a kurtogram [14]. Nevertheless, good agreement was observed between the simulated and experimental results, analysed using time and frequency domain techniques [3, 11–14].

Sawalhi *et al.* [58] also observed that both measured and simulated defect-related transient signals were composed of two impulses: the first was related to the entry of the rolling elements into the defect, and the second, to the exit of the rolling elements out of the defect. They named the phenomenon related to the occurrence of the two impulses as the *double-impulse phenomenon.* Although, the results were reported to have the theoretical background that agrees and supports the findings reported earlier in references [120, 121, 123], Sawalhi *et al.* [58] did not conduct a detailed investigation of the entry- and exit-related vibration signatures. However, later on, they discussed the characteristics of those signatures in a separate publication [124], and subsequently found the double-impulse phenomenon as invalid. These will be described later in Section 4.

The multi-body models reviewed so far [54–62] only considered the inclusion of a single localised defect within a rolling element bearing. In 2010, Patel *et al.* [63] included multiple (two) localised line spalls on both inner and outer raceways in their proposed model for predicting the vibration response of a deep-groove ball bearing. For two raceway defects, two pulses were generated and separated proportionally to the angular separation of the defects. Patel *et al.* [63] presented a 3-DOF shaft-bearing-housing model using lumped masses and springs. The assumptions considered during the development of their model were similar to those mentioned in reference [62]. For the no defect case, in addition to the peaks predicted at the cage frequency f_c, shaft rotational frequency f_s and its harmonics, other peaks were present in the modelled results, which were not discussed. It was shown that for two defects on the outer raceway, the vibration amplitudes of the defect-related frequency components were larger than those obtained for a single defect. However, the amplitudes of the predicted vibration spectra (velocity) of the housing did not match with those obtained experimentally. This highlights the amplitude mismatch reported earlier by several researchers [44, 46, 56, 57, 62].

In 2011, a unique approach was presented by Nakhaeinejad *et al.* [65] for modelling the vibration response of a deep-groove ball bearing due to localised line spalls using vector bond graphs [254]. They developed a 33-DOF multi-body dynamic model of a bearing with nine balls and two rings (outer and inner) considering the translations in the radial (global Cartesian x- and y-directions) and axial (z-direction) planes. Unlike the majority of the multi-body models, the model by Nakhaeinejad *et al.* [65] incorporated the slippage of the rolling elements [49], and their inertial and centrifugal effects. Various widths and heights of the localised defects were modelled on the outer raceway, inner raceway, and one of the rolling elements. The validation of the modelled results was reportedly achieved by comparing them with experimental measurements. Nakhaeinejad *et al.* [65] reported that higher amplitudes are generated for larger defects.

Zhao *et al.* [67] used a commercial multi-body dynamics software package, RecurDyn [255], to model a rolling element bearing having localised line spalls. As their objective was to present a technique for estimating the size of a localised defect [76, 124], they did not provide sufficient details to fully understand the modelling work. Although it was shown that the simulated results agreed well with those of the experimentally measured data taken from the bearing data centre at CWRU [251], the actual modelling process could not be followed due to insufficient details provided in their paper [67].

Extending the work of Sawalhi *et al.* [58, 80], in 2014, Petersen *et al.* [68] reported on the development of an analytical multi-body dynamic model to predict the vibration response of a bearing having raceway defects that include line and extended spalls. Most of the assumptions considered in the model [68] are similar to those in references [58, 80]; however, a few modifications were made to the model to improve the prediction of the vibration response of the bearing. Compared to a single resonance-changer in the earlier model [58] that predicts a high-frequency response of the bearing in one radial direction only (global Cartesian y-direction), an additional mass-spring-damper system attached to the outer raceway was incorporated in the model presented in reference [68] to enable predicting the resonant response in x- and y-directions. The global damping included in the model by Sawalhi *et al.* [58] via a viscous damper attached to the inner ring was replaced by lubrication film damping at the rolling element-to-raceway contact interfaces in the model by Petersen *et al.* [68]. The model [68] also presents an extension of the previously developed model of a defective single-row bearing [58, 80] to a double-row bearing. Inspired by the insights gained from the results of the explicit dynamics FE modelling of a defective rolling element bearing by Singh *et al.* [76–79], the work in reference [68] also presented the quasi-static load distribution and varying stiffness of a radially loaded double-row bearing with a raceway defect. Although the analytical quasi-static load distribution has been included in previous models [53–55, 57–59, 62–66], the authors did not present the distribution on the rolling elements within a bearing. It is shown that the modelled results in reference [68] agree favourably with the measured data presented in reference [58].

Recently, an analytical model to predict the vibration response of a defective rolling element bearing has been reported by Moazenahmadi *et al.* [69]. Unlike the models reviewed above, a unique feature of the model in reference [69] is modelling the finite size of the rolling elements; that is, not point masses as considered in others [57, 61, 65, 66, 68]. Based on the understanding of the physics of the rolling elements traversing a raceway defect through the analysis of the rolling element-to-raceway contact forces by Singh *et al.* [76, 77, 79], the model in reference [69] estimated the trajectory of the rolling elements as they traverse the defect. The high-frequency response of the outer ring of the bearing was chosen to resonate at 10 kHz using a mass-spring-damper system as was considered in previous models [58, 68]. The modelled vibration response agreed favourably with the measured data. In addition to the high-frequency impulsive signals generated at the exit of the rolling elements from the defect [76–79], the model [69] also predicted the low-frequency signals at the entry of the rolling elements into the defect. Such characteristics of the vibration signals have earlier been measured by several researchers [120, 121, 123, 124], and modelled by Singh *et al.* [76–79] using an explicit dynamics FE model of a rolling element bearing having a localised outer raceway defect. A review of the FE models is provided in the next section.

2.4. FE models

The use of analytical and theoretical methods often involves several assumptions and simplifications, which for the previous models, were discussed during their review presented above. Unlike the analytical models, one can minimise the assumptions in FE methods and achieve comparatively better results; however, one has to still assume values for parameters, such as material model, material properties, solver time integration (time-stepping) scheme, damping, and friction, in addition to adequately discretising a model into finite elements so as to accurately model its structural response. This section is concerned with those numerical models that use either commercial FE codes or a combination of analytical and FE codes in order to simulate the response of a rolling element bearing or associated bearing structure due to localised bearing defects. Commercially available FE codes can be classified on the basis of their solver time integration schemes. These schemes include *implicit* [256–263] and *explicit* [261, 264–274] time integration methods. Based on the implementation of the time integration methods, FE models available in the literature for studying various aspects of rolling element bearings, can be broadly categorised into *implicit static* and *explicit dynamic* models. A review of these models is provided in the following sections.

2.4.1. Combination of analytical and implicit FE models

Kiral *et al.* [70, 71] simulated the vibration response of a bearing structure (pedestal — a plummer block), which houses a ball bearing with and without a defect. Although the concept of mathematically generating the periodic defect-induced impulse-train forcing model to simulate the impulsive force as a result of ball–defect interaction was not new, the output of the model was provided as an input to a commercial FE software package, I-DEAS [275]. The outer ring of the bearing and structure were modelled as a rigid assembly using I-DEAS. A localised defect on the outer raceway was modelled by simply amplifying the magnitudes of the radial forces at two adjacent nodes considered to represent the edges of the defect; the depth of the defect was not considered. The mathematical logic behind the values of the amplification factors was not discussed; however, they were chosen to be 6 [70] and 10 [71]. The width of the localised defect was chosen to be the width of two neighbouring nodes as a result of the discretisation of the assembly structure into finite elements. While a single defect was simulated in their former model [70], Kiral *et al.* simulated multiple defects (two, three, and four) on the outer raceway, located at the angular separation of 90°, in their latter model [71]. Standard condition-based monitoring techniques, time (root mean square (RMS) value and kurtosis [3]) and frequency domain (envelope analysis [211, 212]), were applied to the FE modelling results for verification purposes.

2.4.2. Implicit static FE models

In the context of this paper, *implicit static* FE models refer to those models that use a certain type of commercial FE software package that are typically used to analyse the static stress and load distribution within rolling element bearings. A few examples of the FE software packages that have implicit solvers are ANSYS [276], Abaqus [277], ADINA [278], ALGOR [279], I-DEAS [275] and NASTRAN [280].

For the case of non-defective rolling element bearings, a number of researchers [281–297] have conducted FE modelling studies using the aforementioned software packages to investigate the following static parameters — stresses at the rolling element-to-raceway contact interfaces, rolling element-to-raceway contact forces, load-deflection relationships, load carrying capacity of rolling elements, stiffness matrix calculation, and fatigue life. As the models in references [281–297] do not include a defect within the bearing models, they are not directly relevant to the current paper, and therefore, are not reviewed here. However, in reference [286], a transient dynamic FE simulation using ANSYS [276] is presented to predict the vibration response due to a localised defect located at the outer raceway of a bearing. The FE model did not include any other component of a bearing except half of the outer ring structure. In a transient analysis, loads have to be manually defined as a function of time, and the load-versus-time curve has to be divided into suitable load steps. The force-versus-time curve presented in reference [286] was used to simulate a change in the rolling element-to-defect contact force similar to that of a square wave-like pattern with vertical step responses at the edges of the defect — representing a step decrease and increase in the contact force at the leading and trailing edges, respectively. The change in the contact force at the edges of a bearing defect is a complex mechanism, which is characterised by: 1) gradual de-stressing of the rolling elements at the leading edge of a defect causing a low-frequency vibration response [76, 77, 79, 120, 121], and 2) impulsive re-stressing of the rolling elements at the trailing edge of a defect causing multiple (short-duration) force impulses, leading to a high-frequency vibration response [76–79]. The change in the contact force is more complex than a square wave-like function and therefore, the work in reference [286] does not represent an accurate simulation of bearing dynamics.

2.4.3. Explicit dynamic FE models

In the context of this paper, *explicit dynamic* FE models refer to those models that were developed using explicit dynamic FE software packages; for example, LS-DYNA [298], ANSYS Autodyn [299], Abaqus/Explicit [277], and NASTRAN Explicit [280]. These are commercial FE packages that use an explicit time integration scheme [261, 264–274] during the solution phase to solve for time-varying acceleration, velocity, and displacement results.

As for the case of implicit models [281–297], explicit FE models for non-defective rolling element bearings have also been developed [300–303]. These models simulate deep-groove ball bearings, and compare the numerically estimated stress distribution results, obtained using LS-DYNA [298], at the rolling element-to-raceway contact interfaces, with the analytical results obtained using the classical Hertz theory of elasticity [134–136].

Only five publications [72–76] have been found during the survey of the literature that are concerned with modelling the time domain vibration response of rolling element bearings having localised defects using an explicit FE software package [298]. A critical review of these FE models is provided below.

Shao *et al.* [72] presented a 3-D dynamic FE model of a deep-groove ball bearing that was solved using LS-DYNA [298]. It was assumed that the bearing was installed in a structure (pedestal), where the model of the bearing pedestal was similar to the one presented by Kiral *et al.* [70, 71]. Shao *et al.* [72] modelled a same-sized defect on the outer raceway, inner raceway, and one of the rolling elements. However, the size of the defect was not mentioned. The numerically obtained time-varying acceleration results at two nodes, located on the bearing structure, were shown for four simulations: 1) no-defect, 2) an outer raceway defect, 3) an inner raceway defect, and 4) a rolling element defect. While one of the nodes (referred to as *P1*) was located at the 6 o'clock position in close proximity to the outer ring of the bearing, the other (referred to as *P2*) was located in a mounting hole of the pedestal, at a horizontal distance of approximately 60 mm from *P1*. The results presented in reference [72] showed that the magnitude of the acceleration was highest for the outer raceway defect followed by the inner raceway defect, and lowest for the rolling element defect. It was also found that, for the outer raceway defect simulation results, the magnitude of the acceleration signal was significantly lower at *P2* in comparison to *P1*. Because the node at *P1* was in close proximity to the outer raceway defect, the low level of the acceleration signal at *P2* showed that the defect-related impulsive energy attenuates as the output location is moved away from the defect location. Standard time domain statistical parameters, such as RMS, peak value, and kurtosis [3] were compared for the four numerical simulations. It was reported [72] that the values of the parameters were highest for the outer raceway defect followed by the inner raceway defect, and lowest for the rolling element defect. Reference [72] was presented at a conference, and no further details were provided, such as loads and boundary conditions, and did not compare the simulation results with experimental data.

Guochao *et al.* [73] presented a 3-D FE model of a deep-groove ball bearing having a localised defect on its outer raceway. The model was solved using LS-DYNA [298], and the time-varying acceleration, velocity, and displacement results at three nodes located on the outer ring were shown. The nodal locations were: 1) either at the defect or in close proximity to the defect (although neither the nodal location nor the defect was shown in the model), 2) 90° to nodal location '*1*', and 3) 180° to nodal location '*1*'. As the modelling results were not compared with experimental results, Guochao *et al.* [73] validated the simulation results by comparing the numerical outer raceway defect frequency f_{bpo}, (obtained by conducting a Fast Fourier transform (FFT) [210] on the time domain acceleration results) with that of the analytically estimated kinematic defect frequency (refer to Appendix A). Although it was shown that the numerical and analytical f_{bpo} estimates matched reasonably well with each other, the FE model [73] and results have ambiguities that are discussed below.

It was mentioned that the outer ring was modelled as rigid and all the degrees of freedom, translations in the global Cartesian x-, y-, and z-directions, of the nodes located on the outer ring were translationally constrained (i.e. fixed). However, the nodal acceleration, velocity, and displacement results at the aforementioned three nodes located on the outer ring were shown to be varying with time, which contradict the applied boundary conditions.

The magnitude of the numerically estimated time-varying nodal acceleration results for the nodes located at the outer ring were of the order of 10^7 g [73], which is unrealistically high. One of the reasons for such high acceleration magnitudes is due to modelling the outer ring as a rigid body, which may have resulted in the over-stiffening of the bearing model; in the context of FE models, rigid bodies cannot undergo bending or flexural deformation as is the case for the multi-body models in references [53–65, 68, 69], except for the models in references [66, 67]. The other reason for such high acceleration magnitudes is that the model did not include structural damping.

The bearing model by Guochao *et al.* [73] did not have axial and radial clearances. Although not discussed, the pictorial presentation of the stress distribution at the rolling element-to-raceway contact interfaces, Figure 2 in reference [73], does not seem to provide realistic information. This is because, in the case of zero radial clearance, the extent of the load zone is typically 180° around the circumference of the outer and inner rings; that is, ±90° from the point where the radial load is applied [2, pages 235, 239]. This implies that the rolling elements located within the 180° radial load zone extent should have the applied radial load distributed as per the well-developed analytical static solution [2, pages 234–237]. However, from the pictorial presentation, there were three loaded rolling elements, whereas the correct number should have been at least four as per the static load distribution solution [2, pages 234–237].

In addition to the aforementioned ambiguities and/or errors, Guochao *et al.* [73] did not provide several details, which are necessary to clearly understand the modelling work. These include the following:

- Modelled defect — neither the shape of the modelled defect nor the precise location of node '*1*' was clearly mentioned; node '*1*' was mentioned to be either located at the defect or in close proximity of the defect.
- Material model and behaviour — except mentioning that the outer ring was modelled as a rigid body, it was not mentioned whether the remaining components within the model of the bearing, such as inner ring, rolling elements and cage, were modelled as rigid or flexible bodies.
- Friction — it was not mentioned whether friction between the rolling elements and the raceways was applied.
- Damping — it is not clear whether damping was included in the FE model.

Despite the ambiguities, the model in reference [73] appears to be the first in the literature to present an explicit dynamics FE modelling of a defective rolling element bearing.

Liu *et al.* [74] presented a 3-D FE model of a deep-groove ball bearing with the aim of studying the effect of the shape of a localised defect on the vibration signatures. Three shapes of localised defects were modelled on the outer raceway of the bearing — rectangular, hexagonal, and circular. The model was solved using LS-DYNA [298], and the effects of various defects were studied using standard time domain statistical parameters, such as RMS, crest factor, and kurtosis [3]. It was mentioned that while the numerically modelled vibration, displacement, response of the inner ring was mainly influenced by the shape of the localised defects, it was also slightly affected by the radial load, axial load, and shaft speed. Although the model presented by Liu *et al.* [74] is an improvement over the one in reference [73], the model has a few limitations that are discussed in the following paragraphs.

The outer surface of the outer ring was modelled as a rigid surface, and all the six degrees of freedom, translational and rotational, for all the nodes located on the outer surface of the outer ring were constrained. Although not mentioned by Liu *et al.* [74], it is likely that it was done to simulate a rigid support along its circumference, such as a bearing mounted in a housing or pedestal. Also, the purpose of translationally constraining the outer ring was to prevent it from rotating during the simulation, as frictional contact interaction with the rolling elements can cause the outer ring to rotate, which is fundamentally incorrect for the simulated rotating-inner-race-fixed-outer-race configuration. Modelling the outer surface as rigid would cause over-stiffening of the outer ring and constraining the outer ring causes incorrect load distribution on the rolling elements [76, 79], which consequently can affect the vibration response, as the (loaded or stressed) rolling elements interact with the defective surface.

Liu *et al.* [74] presented two types of validation of the numerical modelling results:

1. The *first validation* was related to simply comparing the numerical estimate of the BPFO (obtained after the implementation of the FFT on the modelled velocity time-traces) with the analytically estimated defect frequency: this type of validation has not only been followed for previous FE models [72, 73], but also for the aforementioned multi-body models [53–69]. However, prior to demodulating the numerical velocity time-traces using the envelope analysis technique [211, 212], they were low-pass filtered, with a cut-off frequency of 500 Hz. It is interesting to note that the value of the cut-off frequency was mentioned as 500 Hz in the main text; however, in Figure 2 in reference [74], it was mentioned as 800 Hz. Nevertheless, low-pass filtering of the modelling results eliminates the characteristics of the defect-related impacts, which are essentially impulses of short-duration [76–79]; that is, the defect-related impulsive signals contain a significant amount of energy in the high-frequency region.
2. The *second validation* was related to comparing the shape of the numerically obtained acceleration waveform with the experimental results. While the simulated acceleration results were low-pass filtered, with a cut-off frequency of either 500 Hz or 800 Hz, surprisingly the experimentally measured acceleration results were low-pass filtered, with a cut-off frequency of 2000 Hz. Although the comparison of the shapes of the waveforms for the numerical and experimental results showed some resemblance, the amplitudes were significantly different — the amplitude of the experimentally measured acceleration data (after low-pass filtering) was less than 100 g compared to approximately 4,000 g for the numerically modelled results (after low-pass filtering). One of the reasons for such a high magnitude could be the over-stiffening of the outer ring, as transforming its outer surface to rigid prevents the ring from flexurally deforming. As noted previously, the amplitudes of the numerically modelled acceleration time-traces shown in reference [73] were of the order of 10^7 g, which are unrealistic. As mentioned earlier, the amplitude mismatch problem has also been reported for several multi-body modelling results [44, 46, 56, 57, 62–64].

In addition to the above-listed concerns, Liu *et al.* [74] did not provide the following details:

- Nodal location of the numerical results — for various cases of the numerical simulations, the time-varying displacement, in the global Cartesian y-direction (the displacement in global x-direction was constrained), at the centre of the inner ring was shown. As there was no mention of a shaft in the FE model and the centre of the bearing model was hollow, the location of the displacement results is unclear.

- Application of the low-pass filter to the numerical results — it is unclear whether the numerically modelled displacement results were low-pass filtered before estimating the time domain statistical parameters; RMS, crest factor, and kurtosis.

- Noise in the simulation results — it was mentioned that the surfaces within the bearing model were smooth and no noise was generated during the numerical simulations. However, it was unclear why they need to low-pass filter the results to remove high-frequency noise. It has been demonstrated by Singh *et al.* [76–79] that a numerical solution estimated using LS-DYNA generates a significant amount of numerical noise, which is an inherent feature of its solution phase [304, page 1110]. Using their explicit dynamics FE model of a defective rolling element bearing, they explained that the circular rolling elements and raceways transform into multi-point polygons during the discretisation of the model into finite elements. The rolling of the *polygonised* rolling elements between the raceways generates tonal noise at frequencies, which are a function of the size of the finite elements, diameter of the raceways and the rotational velocity of the rolling elements [76–79].

- Damping — it is not clear whether damping was included in the FE model.

- Radial and axial clearances — it was not mentioned whether the clearances were included within the model.

Utpat [75] developed a 3-D FE model of a deep-groove ball bearing with localised defects on the outer and inner rings. He discussed the effects of various sizes of defects on the magnitudes of the numerically modelled acceleration at a node located on the outer surface of the outer ring. The FE model was solved using LS-DYNA, and it was shown that the vibration levels increased with increasing defect size and shaft rotational speed. Although the numerical results were shown to be in close agreement with experimental results, Utpat [75] did not provide important details necessary to verify the presented modelling results. The following paragraphs describe some of the potential issues with the work presented in reference [75].

The inclusion of the cage within the FE model of the bearing was not mentioned. The function of a cage in a bearing is to retain the rolling elements, and that is why, it is often referred to as a *retainer*. Without the presence of a cage, the rolling elements will interact with each other causing bearing lockup. It is possible that the centre of the rolling elements could have been connected and rotated, thereby, constraining their centrifugal and inertial effects, but it was not mentioned in the publication.

Utpat [75] described the discretisation of the bearing model (outer ring, inner ring, and rolling elements) into nodes and elements (Figures 2a and 2b in reference [75]). Although the element mesh size was not mentioned, the meshing of the components was coarse, especially, the tetrahedral mesh of the outer ring. Singh *et al.* [76–79] showed that it is not possible to achieve smooth rotation of the rolling elements about their own axes with a coarse mesh. They discussed that the meshing at the rolling element-to-raceway contact interfaces within the load zone [2, pages 234–237] must be sufficiently fine so that the contact between the rolling elements and raceways of a bearing can be maintained at all times. This is because if the rolling element-to-raceway contact is lost, the transmission of forces (load) between the components will be incorrect, which can affect the vibration response of the bearing [76–79]. It is generally recommended to use at least 20 elements-per-wavelength (EPW) for a transient dynamic structural analysis [305, Chapter 5]. However, for their FE model of the bearing, Singh *et al.* [76–79] showed that it was necessary to use 97 EPW, which is nearly 5 times the recommended EPW criterion.

Utpat [75] showed the numerical acceleration time-traces estimated at a node located at the outer surface of the outer ring. For the case of the simulated outer raceway defect, the limits of the instantaneous acceleration levels were approximately $\pm 20 \times 10^4$, but without units (Figure 4 in reference [75]). For the case of the modelled inner raceway defect, the limits of the instantaneous acceleration levels were approximately $\pm 15 \times 10^4 \quad \mathrm{m/s}^2$ (Figure 6 in reference [75]), which is 25% less than the outer raceway modelling acceleration levels. The frequency domain representation of acceleration results for both outer and inner raceway defects were shown on a linear scale, and the amplitudes at the fundamental outer and inner defect frequencies, f_{bpo} and f_{bpi}, respectively, were mentioned as $905\,\mathrm{mm/s}^2$ and $693\,\mathrm{mm/s}^2$, respectively. Given that these amplitudes are approximately 25% different from each other, it is highly likely that the units for the numerically modelled acceleration time-traces related to the outer raceway defect simulation (which are not mentioned in reference [75]) could also be $\mathrm{m/s}^2$. Nevertheless, even for the case of the modelled inner raceway defect, the instantaneous levels of the acceleration time-traces, $\pm 15 \times 10^4\,\mathrm{m/s}^2$ (approximately $\pm 15,000\,\mathrm{g}$), are unrealistically high. It is interesting to note the instantaneous amplitudes of the experimentally measured acceleration data were between $\pm 100\,\mathrm{m/s}^2$ (approximately $\pm 10\,\mathrm{g}$). The excellent match between the numerical and experimental results shown in Figure 11 in reference [75] is surprising. It should also be noted that unrealistically high acceleration levels of $10^7\,\mathrm{g}$ [73] and 4,000 g [74] were also reported in the previous modelling results discussed above.

In addition to the aforementioned concerns, the following details were not provided by Utpat [75], which are necessary to understand the modelling work:

- Material behaviour — it was not mentioned whether the components of the bearing model, outer ring, inner ring and balls, were modelled as rigid or flexible bodies.

- Loads and boundary conditions — the boundary conditions applied to the model were not described. It is important to know how the outer ring was kept stationary, because in the event of rotation of the inner ring and rolling elements, the outer ring would also rotate, if not constrained. However, the outer ring cannot be translationally constrained in either x-, y- or z-directions [76, 78, 79], as it will cause an incorrect load distribution, and consequently affect its vibration response. It should be noted that Liu *et al.* [74] modelled the outer surface of the outer ring as rigid so it can be fixed in its position. However, this resulted in the over-stiffening of the outer ring, which might have resulted in the very high numerical acceleration levels of 4,000 g compared to the experimental acceleration levels of less than 100 g [74].

- Friction — it was not mentioned whether friction between the rolling elements and the raceways was applied.

- Clearance — it was not mentioned whether any clearance between the rolling elements and raceways was included within the model.

- Defect size — despite the model being 3-D, the defect sizes were mentioned as 0.25 mm, 0.5 mm, 1 mm and 2 mm. It is not clear whether these figures represent length, width, or height.

Singh *et al.* [76] developed a 2-D explicit dynamics FE model of a rolling element bearing that included a line spall on its outer raceway. The model was solved using LS-DYNA [298]. Unlike previous FE models [73–75], which compromised performance by modelling either the whole outer ring as rigid or its outer surface as rigid, the model by Singh *et al.* [76] included all the bearing components (outer ring, inner ring, rolling elements, and cage) as flexible bodies. This facilitates a more accurate representation of the bearing stiffness and the vibration response of the bearing. The results in reference [76] showed that the instantaneous amplitude of the simulated vibration signals agreed favourably with measured data, which is in contrast to the significant amplitude-mismatch between the modelled and measured results for previous FE models [73–75] and multi-body models [56, 57, 62–64].

Singh *et al.* [76] also presented an in-depth analysis of the numerically modelled dynamic rolling element-to-raceway contact forces, which has been ignored in previous FE [72–75] and multi-body models [53–68]. Through the analysis of the contact forces, Singh *et al.* [76] showed the gradual de-stressing of the rolling elements as they enter into a raceway defect, and impulsive re-stressing of the rolling elements as they exit out of the defect. An important outcome of their work is that a burst of multiple, short-duration, force impulses is generated during the re-stressing of the rolling elements, which occurs in the vicinity of the trailing end of a defect. They showed that during the re-stressing of the rolling elements, they alternatively strike the outer and inner raceways causing multiple force impulses in contrast to a single force impulse as has been previously considered in references [43–49, 56, 67, 124].

The simulated results by Singh *et al.* [76] also confirmed the generation of low-frequency vibration signals associated with the de-stressing of the rolling elements upon their entrance into a bearing defect. Although the low-frequency characteristics of the de-stressing event have been measured by a few researchers [120, 121], previous multi-body analytical models [43–64, 66–68] could not predict this event. Previous FE models [72–75] also did not report on the signals related to the de-stressing event: similar to the multi-body models, the emphasis of the FE models was to predict the defect-related (re-stressing) impulses and validate the modelling results through an envelope analysis [211, 212]. Singh *et al.* [76] showed that although a rolling element can strike the surface of a defect and generate a low amplitude acceleration signal, a much higher acceleration signal is generated when the rolling elements are re-stressed between the raceways.

3. Extended defects

An *extended defect* can be characterised as a defect that is larger than a localised defect (for example, its size can be greater than the spacing between two rolling elements), but smaller than a distributed defect (for example, waviness is generally along full raceways). Once a localised defect (a spall) is created on either raceway of a bearing due to surface fatigue [3–5, 129–132], the continuous and repetitive passage of the rolling elements over the spall results in the generation of impulsive (contact) forces during the re-stressing of the rolling elements [76–79]. This cyclic operation wears the edges, especially the trailing edge, of the spall causing it to gradually grow or expand in size, and results in the generation of an extended defect [306].

In contrast to localised [43–79] and distributed defects [81–119], extended defects have received much less attention. Only two publications [68, 80] could be found in the literature that discuss the vibration modelling of a rolling element bearing with an extended defect, and are discussed below.

3.1. Nonlinear multi-body dynamic models

Sawalhi *et al.* [80] extended their previous work [58] on the vibration modelling of a rolling element bearing with a localised defect (discussed in Section 2.3.3). They presented a combined nonlinear multi-body dynamic model for gears and bearings in which an extended defect on either of the two raceways can be studied in the presence of gear interaction. They characterised the extended defects as faults that extend beyond the spacing between two rolling elements, and have been smoothened by the successive passage of the rolling elements, so that no sharp impulses are generated, and no defect-related frequencies are detected in the envelope (demodulated) spectrum. They referred to the extended defects as *rough surfaces*. They modelled the inner and outer rings as rigid bodies, and the rolling element-to-raceway interfaces as nonlinear contact springs. The mass of the rolling elements, and their inertial and centrifugal effects were not considered due to the low run speeds used in the experiments. Slippage of the rolling elements [49] was included in their model to obtain a closer resemblance between the predicted and measured vibration spectra. Damping was included via a grounded damper attached to the inner raceway. An additional mass-spring-damper system, resonant-changer, representing a typical high-frequency bearing resonance (15 kHz) was attached to the outer raceway. The objective of the work presented by Sawalhi *et al.* [80] was the differential diagnosis of gear and bearing defects [49–51], which was achieved by utilising the difference in the cyclostationary properties of the gear and bearing signals [214, 215, 218]. The simulation results included acceleration signals for inner and outer raceway extended spalls, and their corresponding squared envelope [48] and cyclic spectral densities [17, 216, 217]. The results were compared with experimental data for a bearing where extended faults were etched on both of its raceways, and good similarity between the two results was achieved. Due to the rough surface characteristics of the extended defect, the use of the envelope spectrum did not identify the inner race defect frequency f_{bpi}, whereas the spectral correlation function enabled detection of the defect frequencies.

Petersen *et al.* [68] further modified the work of Sawalhi *et al.* [58, 80] to improve the prediction of the vibration modelling of defective bearings. Reference [68] included the modelling of the vibration response of a rolling element bearing with both localised and extended defects. A review of the model has already been provided in Section 2.3.3. Petersen *et al.* [68] showed that for an extended spall with large wavelength surface roughness (waviness) features, the stiffness of the bearing changes slowly than a localised narrow line spall that leads to the low-frequency parametric excitation of bearing structure. For the extended spall, the defect-related frequency components due to the excitation were clearly visible in the velocity spectra.

4. Defect-related vibration characteristics

The main objective of the models, impulse-train [43–52], multi-body [53–69], and FE models [70–75] (except [76]), reviewed so far was to predict the significant vibration frequency components; fundamental, harmonics, and associated sidebands, related to localised surface defects in rolling element bearings. The emphasis on investigating the change in the characteristics of bearing vibration signals at the edges of a

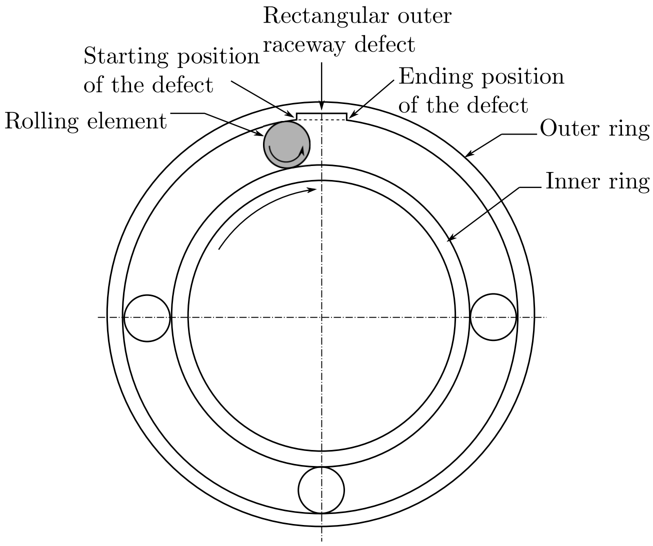

Figure 2: A 2-D schematic of a rolling element bearing model comprising an outer ring, an inner ring, a few rolling elements, and a geometric rectangular defect on the outer raceway.

defect, leading and trailing, has been far less compared to the efforts expended on the development of the aforementioned models. On the one hand, as point spalls were considered by the majority of researchers [43–51, 53, 56, 57, 59, 61, 62], it is logical to say that the change in the characteristics of vibrations at the two edges of point spalls could not possibly be studied. On the other hand, a few researchers have modelled localised defects as line [52, 54, 55, 58, 63, 65, 67–69, 74, 75], circular [60, 64] and elliptical [66] spalls; however, the change in the vibration characteristics was only briefly mentioned in references [58, 65, 67–69] generally in the context of estimating the average size of bearing defects. In contrast, the work by Singh *et al.* [76–79] was focused on the analysis of the rolling element-to-raceway contact forces and their correlation with the bearing vibration signatures generated during the traverse of the rolling elements through a raceway defect. From the analysis of the results from FE simulated contact forces, they [76, 79] also discussed the generation of the low- and high-frequency characteristic vibration signatures generated at the entry and exit of the rolling elements into and out of a raceway defect, respectively.

It is the aim of this section to present a review of existing knowledge corresponding to the characteristics of the vibration response at the leading and trailing edges of a bearing defect.

4.1. Entry- and exit-related transient features

Epps, in his doctoral thesis [120] and a conference paper co-authored by McCallion [121], provided a detailed insight into the characteristics of the vibration response at the two edges of a bearing defect. They measured the acceleration waveforms (time-traces) of ball bearings with three different sizes of localised defects. The defects were artificially etched on the outer and inner raceways, and their sizes ranged from 0.2 mm to 3.0 mm. On the basis of the experimental observations, they hypothesised that the defect-related (vibration) transient, as a result of the traverse of a rolling element over the defect, was essentially composed of two parts or events — first, the entry of the rolling element into the defect, and second, its exit out of the defect. For the ease of relating the entry and exit of the rolling elements into and out of a bearing defect, the leading and trailing edges of a defect are referred to as the starting and ending positions, respectively, in this paper. Figure 2 shows a schematic of a 2-D model of a rolling element bearing comprising an outer ring, an inner ring, a few rolling elements, and a geometric rectangular defect located on the outer raceway of the bearing. The starting and ending positions of the defect are illustrated in the figure.

A figure from Epps's thesis [120] that shows the experimentally measured acceleration of the ball bearing having an outer raceway defect of width 3.0 mm is shown in Figure 3. The two annotations in the figure,

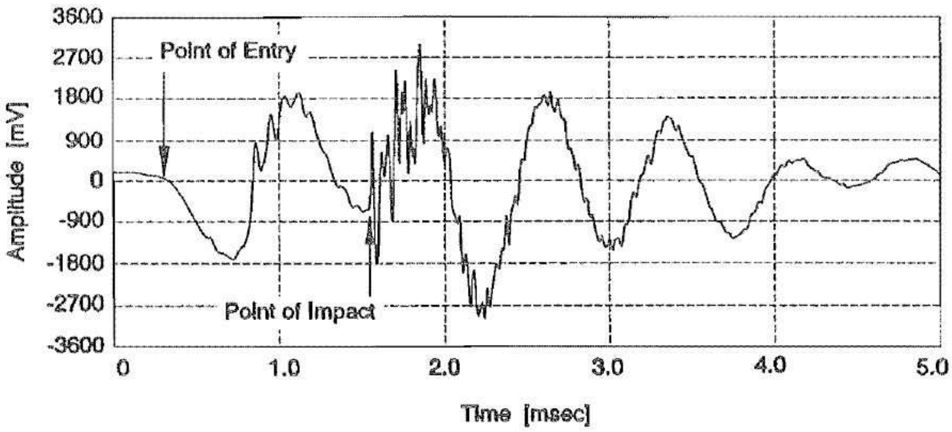

Figure 3: Experimentally measured acceleration response of a rolling element (ball) bearing with an outer raceway defect of 3.0 mm, taken from references [120, 121] (permissions to be obtained).

'*Point of Entry*', and '*Point of Impact*', correspond to the entry and exit of a rolling element into and out of the defect, respectively. Epps *et al.* [120, 121] suggested that the entry of the rolling elements into a defect can be considered as a low-frequency event with no evidence of impulsiveness, and in contrast, their exit out of the defect can be considered as a high-frequency impulsive event that can lead to the excitation of a broad range of frequencies, and consequently resonant bearing modes. They found that the time difference between the vibration signatures at the entry and exit points in the measured acceleration signals approximately correlate with the size of the defects. The correlation, therefore, successfully supported the distinction of the entry- and exit-related events, and also transients, as the rolling elements traverse through the defects.

Singh *et al.* [76, 79] have modelled the vibration response of a rolling element bearing having a localised line spall on its outer raceway. A spectrogram plot from their numerically modelled vibration response of the bearing, shown in Figure 4 [79], clearly highlights the distinct low-frequency de-stressing and high-frequency re-stressing of the rolling elements as they enter into and exit out of the defect, respectively. The energy of the de-stressing event is concentrated below 3 kHz, whereas the impulses generated during the re-stressing of the rolling elements appear to be characterised mainly by energy in the high-frequency band of 10–25 kHz.

Previous experimental studies [10, 307] have suggested that as the width of a bearing defect increases, the magnitude of the defect-related vibration impulses increases, but the characteristic shape of the impulsive signals is not affected. Similarly, for increasing rotational speed, the magnitude of the impulses increases, but their shape does not change. However, Epps [120] found that not only the magnitude of the impulses, but also their characteristic shapes were influenced by the radial load, rotational speed, and the position of a defect with respect to the bearing load zone [2, 76, 79, 205–208].

For condition-based monitoring of machinery, Dowling [123] highlighted the potential need for the application of non-stationary analysis, such as wavelet transform [3, 308, 309] and Wigner-Ville distribution [308, 310–312]. He discussed the non-stationary characteristics of machinery-based vibration signatures, generally measured in practice, with attention focused on the stochastic nature of signatures associated with defective bearings. He presented a recorded waveform from a helicopter gearbox bearing, having an outer raceway defect, from an earlier reference [122], and briefly described the nature of the defect-related transient signal. The waveform is shown in Figure 5 for discussion purposes.

With regards to the results in Figure 5, it was mentioned that a rolling element took approximately 0.3 milli-seconds (ms) to traverse through the outer raceway spall. The time separation of 0.3 ms is shown in the figure: the two ends of the time separation marker correspond to the aforementioned entry- and exit-related events. It was described that the transient vibration commenced as the rolling element entered

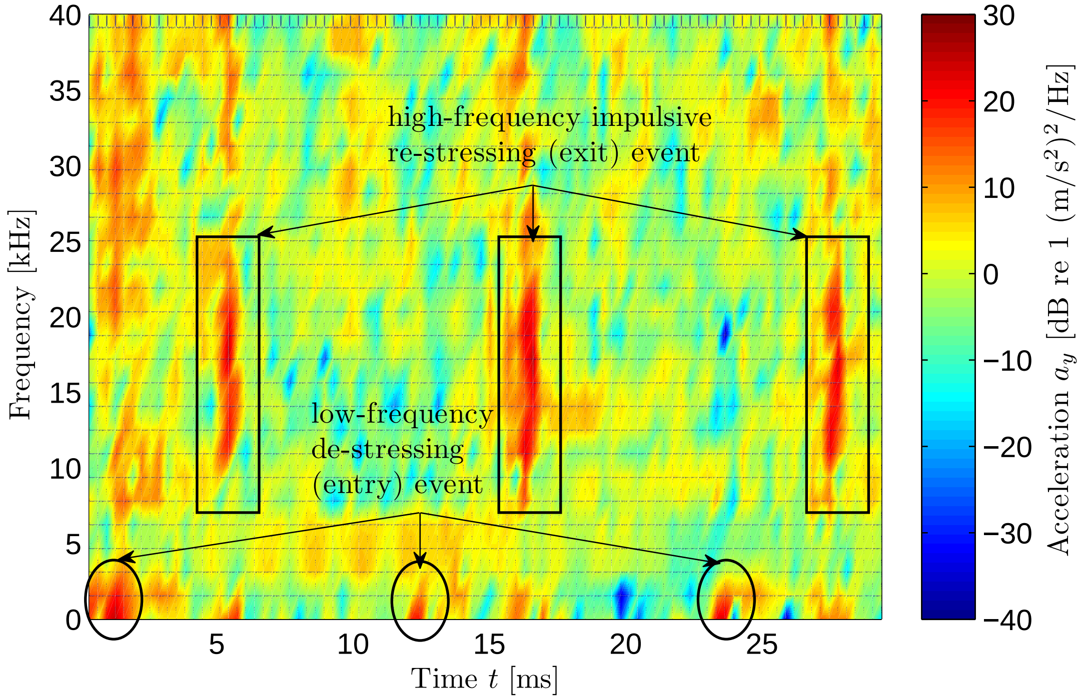

Figure 4: A spectrogram of the numerically modelled acceleration a_y time-trace, highlighting the low-frequency de-stressing and high-frequency re-stressing events using the elliptical and rectangular markers, respectively [79].

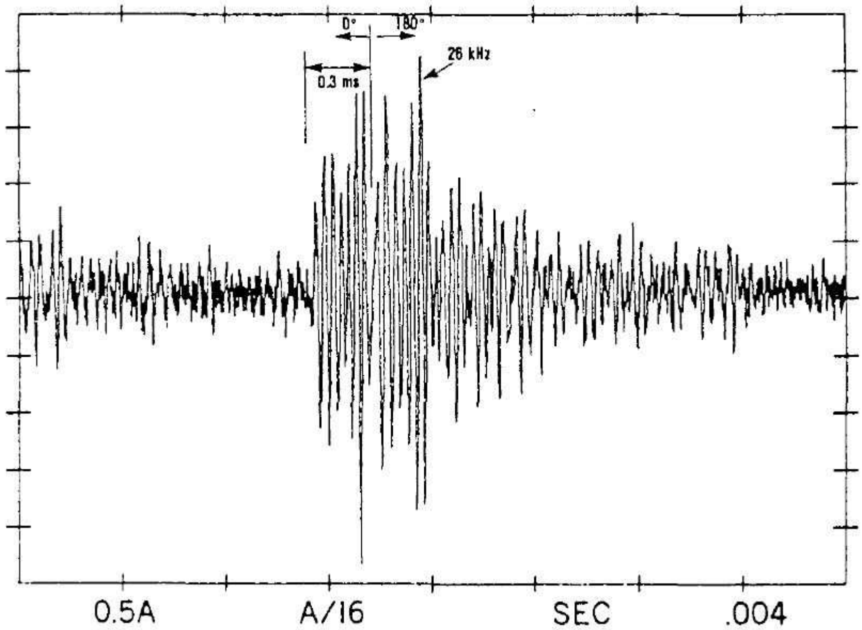

Figure 5: Band-pass filtered accelerometer time-trace from a helicopter gearbox bearing with an outer raceway spall, taken from references [122, 123] (permissions to be obtained).

the defect, and upon its exit from the defect, an impact was generated that interfered with the transient that occurred at the beginning, resulting in a 180° phase shift. Thus, Dowling [123] related the change in the characteristics of the defect-related vibration signatures associated with the entry and exit of the rolling element into and out of the defect, respectively, by a 180° phase-reversal. However, no further discussion about to the charactersitics of the transient vibration response was provided.

Although the results of Dowling [123] (Figure 5) are not as clear as those presented by Epps *et al.* [120, 121] (Figure 3), both represent similar findings — no evidence of impulsiveness at the entry of the rolling element into the defect, and impulse-like signatures at its exit out of the defect.

A careful observation of Figure 5 shows an additional peak after the exit-related impulse; however, the occurrence of the multiple impulses was not discussed [123]. Sawalhi *et al.* [58] initially considered that the occurrence of the two impulses was associated with the entry and exit of the rolling elements into and out of a bearing defect, respectively; however, later on, they retracted their claim [124]. This double-impulse phenomenon is described in the next section.

4.2. Double-impulse phenomenon

Sawalhi *et al.* [58] observed double impulses in the results simulated using their proposed nonlinear multi-body dynamic model for predicting the vibration response of a rolling element bearing having a localised raceway defect. A review of their analytical model [58] has been provided in Section 2.3.3. Interestingly, they also found the presence of double impulses in the experimentally measured results. A figure that compares the measured and simulated results from their work [58], illustrating the presence of double impulses is shown in Figure 6. They mentioned that the time separation of 0.0013 seconds between the two impulses, highlighted in Figure 6, corresponds to the time that a rolling element takes to traverse the width of the outer raceway defect. The close match between the simulated and measured results not only helped Sawalhi *et al.* [58] validate their model, but also provided their results with a firm theoretical background, which appeared to be in agreement with the findings reported earlier by Epps *et al.* [120, 121] and Dowling [123]. On the basis of the agreement, Sawalhi *et al.* [58] considered the two impulses to be associated with the entry and exit of the rolling elements into and out of the defect, respectively. They coined the phrase, '*double-impulse phenomenon*', to represent the occurrence of two defect-related vibration impulses.

From the results presented in Figure 6 [58], it appears that the entry- and exit-related impulses have similar characteristics in terms of their frequency content. In other words, the results in Figure 6 imply that both entry- and exit-related events appear to be characterised by energies in high-frequency regions. This represents a stark contrast to previous results reported by Epps *et al.* [120, 121] and Dowling [123], who suggested that the entry of the rolling elements into a defect is a low-frequency event with no impulse-like characteristics. Although Sawalhi *et al.* [58] did not discuss the characteristics (frequency content) of the double impulses, the results presented in Figure 6 [58] imply that the entry of the rolling elements into a defect may not be a low-frequency event. As will be discussed in the next section, it is possible that there is an error associated with the results shown in Figure 6.

4.2.1. Problems associated with the double-impulse phenomenon

In 2011, Sawalhi *et al.* [124] reported results from a series of laboratory tests conducted on self-aligning double-row rolling element bearings with inner and outer raceway defects. Line spalls of width 0.6 mm and 1.2 mm were artificially manufactured on the raceways, and the tests were conducted at various shaft rotational speeds, ranging from 800 to 2400 revolutions per minute.

In their earlier findings, as discussed in the preceding section (refer to Figure 6), Sawalhi *et al.* [58] mentioned that the time separation of 0.0013 seconds between the two impulses corresponds approximately to the time it takes for a rolling element to traverse the width of the manufactured outer raceway defect of 0.8 mm. Later, they mentioned that the time separation actually corresponds to the time it takes for a rolling element to traverse the half the size of the defect. Furthermore, when they repeated the experiments at various shaft rotational speeds, they found that the time separation between the two impulses did not change [124]. Therefore, unlike their earlier findings [58] that implied that the entry of the rolling elements into a defect may not be a low-frequency event, the recent experimental findings by Sawalhi *et al.* [124]

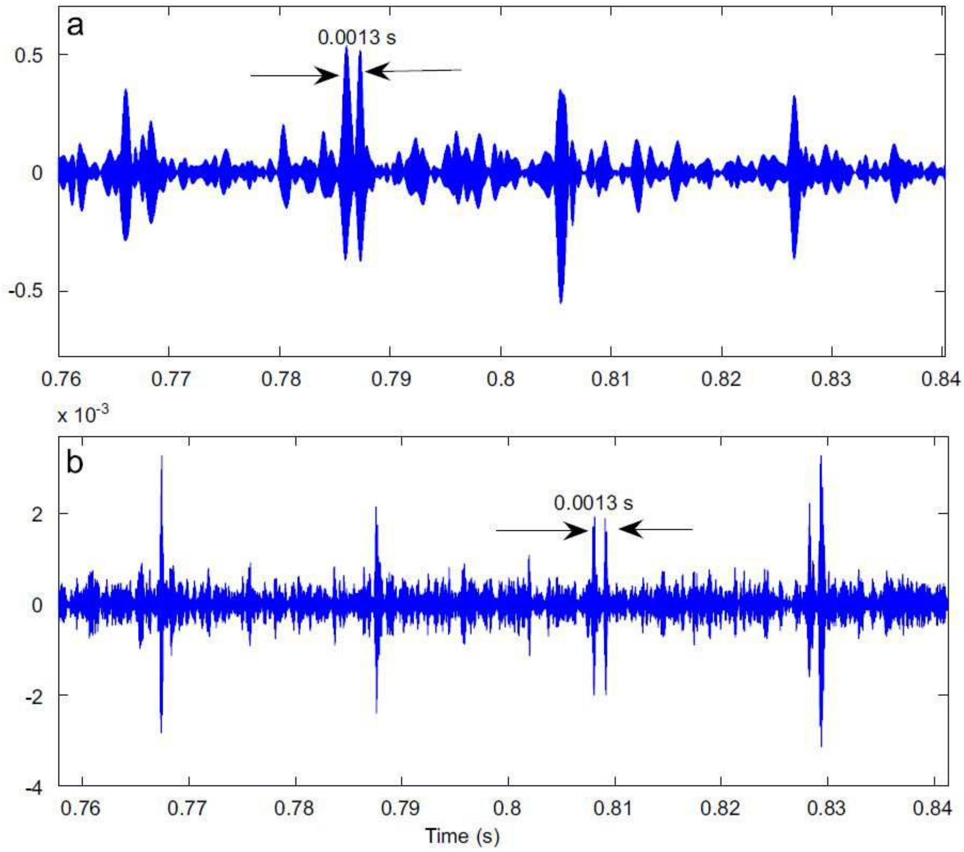

Figure 6: Band-pass filtered signals (one complete rotation of the shaft) with a spall in the outer race, taken from reference [58]: (a) measured, (b) simulated (permissions to be obtained).

correlate with those observed by Epps *et al.* [120, 121] and Dowling [123]; thereby, confirming the entry of the rolling elements into a defect as a low-frequency event.

Invalidating the double-impulse phenomenon, Sawalhi *et al.* [124] suspected that the two impulses could be due to a beating effect related to a small difference in the resonance frequencies of a bearing possibly due to stiffness nonlinearity. From the survey of the literature conducted during the course of this paper, the reason for the occurrence of multiple impulses (as shown in Figure 6 as a result of a single rolling element traversing the defect in typically measured bearing vibration signals is not clearly known. Recently, Singh *et al.* [76] have provided an insightful explanation about the occurrence of the defect-related multiple impulses using the explicit dynamics FE modelling of a defective rolling element bearing as discussed in the next section.

4.3. Physics behind the generation of defect-related impulses

From the analysis of the FE simulated rolling element-to-raceway contact forces and their correlation with the bearing acceleration results, Singh *et al.* [76] showed that defect-related impulses, which are generally observed in measured bearing vibration signals, are generated during the re-stressing of the rolling elements. The re-stressing occurs in the vicinity of the end of a bearing defect as the rolling elements exit out of the defect. They [76] also explained that higher forces and stresses are generated during the exit of the rolling elements from the defect compared to when they strike the defect surface, and hence, could lead to the gradual expansion or lengthening of the defect. These findings show excellent agreement with the experimental study conducted by Hoeprich [306], who investigated the damage progression in rolling element bearings and found that the size of a spall progresses in the rolling direction.

As opposed to the tentative explanation of beating about the occurrence of multiple impulses provided by Sawalhi *et al.* [124], Singh *et al.* [76] showed that a burst of multiple, short-duration, force impulses are generated during the re-stressing of the rolling elements. These force impulses consequently cause multiple vibration impulses that are caused as the rolling elements are compressed between the outer and inner raceways. This is commonly observed in practice in measured bearing acceleration signals, which are subsequently used for bearing diagnosis.

5. Defect size estimation

This section discusses existing knowledge on the estimation of the average size of a defect in rolling element bearings. Similar to the literature on the vibration characteristics at the edges of a bearing defect, the extent of knowledge for estimating the average size of a bearing defect is also limited.

It has previously been mentioned that a defect-related transient is composed of two parts [76, 79, 120, 121]. While the entry-related event is considered to be a low-frequency event, the exit of the rolling elements from a defect is found to be a high-frequency impulsive event. From the results of the FE modelling of a defective bearing and their subsequent comparison with measured data, Singh *et al.* [76, 79] highlighted the distribution of the energies corresponding to the two events — < 3 kHz for the entry- and 10–25 kHz for exit-related events.

Based on the distinct vibration signatures, Epps *et al.* [120, 121] suggested correlating the time difference between the two events as a measure of an average defect size. Singh *et al.* [76, 79] also used the time separation between the entry- and exit-related vibration signatures, and suggested a mathematical formula to approximate the size of a defect.

5.1. Entry- and exit-related vibration models

On the basis of their experimental findings, Sawalhi *et al.* [124] suggested that the entry and exit of the rolling elements into and out of a defect can be described as a step response and an impulse response, respectively. They developed two analytical models in order to represent the two responses. While the resonance frequency of 6500 Hz used for the impulse response analytical model was selected on the basis of the experimental results, no explanation was provided on the selection of the 1084 Hz resonance frequency for the step response analytical model, which was one-sixth of the resonance frequency of the impulse response.

In order to estimate the average size of a bearing defect, Sawalhi *et al.* [124] proposed two algorithms to enhance the vibration signals related to the entry and exit of the rolling elements into and out of a defect, respectively. The first algorithm comprised a joint treatment of the entry- and exit-related transient signals. The signals were first pre-whitened using an autoregressive model [313, 314] in order to balance the low- and high-frequency energies. The pre-whitened signals were then subjected to a complex octave band wavelet analysis (using Morlet wavelets [315, 316]) to allow selection of the best band (or scale) to balance the two events with similar frequency content. The squared envelope [48, 49] was generated next using Hilbert transform methods [317, 318], and finally, a real cepstrum [319–321] was used to estimate the average separation of the entry- and exit-related signatures. The second algorithm treated the entry- and exit-related signatures separately; all the steps mentioned above were separately applied to the vibration responses, so that they could be equally represented in the signal. A mathematical expression for estimating half the actual width of a bearing defect was presented [124]. It was reported to be limited in its capacity to estimate the smallest size of 0.6 mm, but it was proposed that the results would perhaps be more reliable for larger defects.

Zhao *et al.* [67] utilised the combination of empirical mode decomposition [314] and approximate entropy method [322–325] to separate the entry- and exit-related transients. The vibration signals were decomposed into finite components, called as intrinsic mode functions, using the empirical mode decomposition method. The complexity in choosing the appropriate intrinsic mode functions that contain the defect-related entry- and exit-related vibration signatures was demonstrated. Zhao *et al.* [67] compared their signal processing

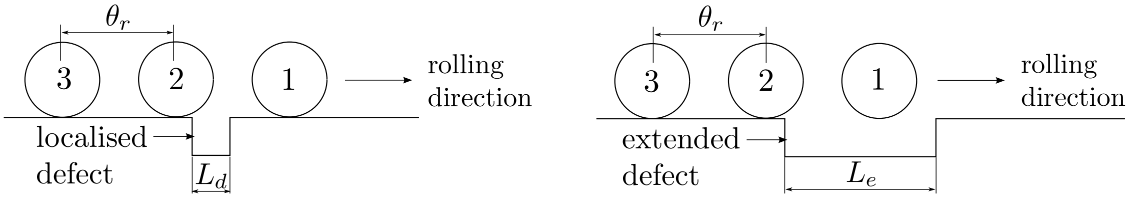

(a) A localised defect whose length L_d is smaller than the angular spacing θ_r between the rolling elements.

(b) An extended defect whose length L_e is greater than the angular spacing θ_r between the rolling elements.

Figure 7: Schematics of a partial defective raceway of a rolling element bearing and a few rolling elements.

algorithms with those presented by Sawalhi *et al.* [124], and reported to be better in representing the separation of the signals.

5.2. Limitations of using time separation between entry- and exit-related vibration signatures as a parameter for defect size estimation

It should be noted that the mathematical expressions for estimating the average size of a bearing defect, developed in references [67, 76, 124], are applicable to those defects whose lengths are smaller than the angular spacing between the rolling elements of a bearing. In other words, the expressions that use time separation between the entry- and exit-related vibration signatures will produce reliable defect size estimates if a rolling element that enters a defect must exit the defect prior to any other rolling element entering and exiting the defect. In the case of extended defects whose lengths extend beyond the spacing between two consecutive rolling elements [80], the consecutive entry- and exit-related events pair will correspond to different rolling elements. In other words, a rolling element may enter a defect, but prior to its exit, other rolling elements will exit out of the defect, resulting in a smaller than actual time separation between the events, and thereby, leading to incorrect estimation of the defect size.

For further clarification of the explanation provided in the preceding paragraph, refer to Figure 7. It shows two schematics of a partial defective bearing raceway and a few rolling elements, labelled as '1', '2', and '3'. In Figure 7a, the length L_d of the localised defect is smaller than the angular spacing θ_r between two consecutive rolling elements, whereas in Figure 7b, the length L_e of the extended defect is greater than the angular spacing θ_r between two consecutive rolling elements. Consider that the rolling elements are travelling from the left to right hand side in both schematics.

In Figure 7a, the rolling element, labelled as '2', will enter into the defect and exit out of the defect, prior to the entry and exit of rolling element '3' into and out of the defect, respectively. In other words, for the case of a localised defect whose length is smaller than the angular spacing between two consecutive rolling elements, the entry- and exit-related vibration signatures are generated due to the entry and exit of a single rolling element into and out of the defect, respectively. In such a scenario, using the time separation between the two distinct vibration signatures, low- and high-frequency, will enable a reliable estimation of the size of a defect.

In Figure 7b, rolling element '1' is already in the defective region. Following the entrance of rolling element '2' into the defect, rolling element '1' will exit out of the defect, prior to the exit of rolling element '2'. In other words, a low-frequency vibration signature is generated due to the entry of rolling element '2' into the defect, whereas a high-frequency signal is generated due to the exit of rolling element '1' out of the defect. Therefore, in contrast to localised defect, for the case of an extended defect whose length typically extends beyond the angular spacing between two consecutive rolling elements, the entry- and exit-related vibration signatures are generated due to the entry and exit of different rolling elements. In such a scenario, it is not practical to use the time separation between the two signals as it will result in an incorrect estimation of a defect size, which would be smaller than the actual defect size.

Recently, Petersen *et al.* [125] showed that a shift in the characteristic frequencies related to the entrance of the rolling elements into a defect can be used to distinguish between defects whose length is smaller and greater than the angular spacing of the rolling elements. They showed that as the size of a defect varies, the stiffness and the natural frequencies of the rigid body modes of a ball bearing assembly vary. Compared to a non-defective bearing, the change occurs more rapidly as the rolling elements enter into and exit out of the defects. The variation in the stiffness subsequently leads to the parametric excitation of the bearing at the defect frequency resulting in the generation of low-frequency events with different characteristic frequencies. The difference can be used to distinguish between the two defects provided the static load on a bearing remains constant. However, the simulation results in reference [125] need experimental validation.

6. Summary of literature

The existing models for predicting the vibration response of rolling element bearings with localised defects have provided an excellent understanding of the defect-related vibration frequency components. Several authors have used analytical, numerical, FE, and a combination of analytical/numerical and FE methods to predict the vibration response of bearings and associated rotor–bearing systems. The characteristics of vibrations at the starting and ending positions of a defect have also been well-established. This section aims to summarise the review of the literature presented in this paper followed by some future research directions in the concluding section.

Impulse-train models. Periodic impulse-train models [43–46] to simulate point defects on the rolling surfaces of a bearing, outer and inner raceways, and a rolling element, provided useful insights into understanding the presence of various discrete frequency components in typically measured bearing acceleration signals. The defect-induced force impulses were generated using the Dirac delta function and a 1-DOF system response. Three typical pulse shapes, rectangular, triangular and half-sine, of finite widths were considered, and their effects on the vibration (line) spectra, including frequencies and amplitudes, were investigated under radial and axial loads [46]. The equi-spaced force impulses of equal amplitude were modelled for the case of a stationary outer raceway bearing defect [45, 46], whereas for rotating inner raceway [43–46] and rolling element defects [45, 46], the amplitude of the impulses was modulated as per the static load distribution [2, 205–208] within a bearing. The periodic impulse-train models were extended [47–51] with the inclusion of the slippage of the rolling elements [48, 49], so as to gain close agreement with typical vibration measurements obtained in practice.

The impulse-train models successfully predict the significant defect-related frequencies (fundamental, sidebands, and harmonics); however, they could not provide a reasonable prediction of their amplitudes. The problem was specifically highlighted by Tandon *et al.* [46] who showed the comparison of the predicted vibration (line) spectra with experimentally measured results; other authors only provided defect periodicities [43, 45]. The problem of amplitude mismatch is largely due to the following factors:

- the mismatch between the mathematically modelled defect-related impulses (rectangular, triangular, and half-sine) and unknown characteristics of actual defect-induced impulses,
- the exclusion of basic bearing components, such as the outer ring, inner ring and rolling elements, and structure from the analytical models compared to measuring the vibration response of a bearing, which is generally installed in some kind of housing, such as a pedestal, and
- the consideration of several assumptions and simplifications during the development of the models.

The amplitudes of the frequency components were also normalised or corrected; however, neither the normalisation factor was provided nor the mathematics behind the normalisation factor were discussed [46].

Nonlinear multi-body dynamic models. Unlike the impulse-train models, the nonlinear multi-body dynamic models [53–69, 80] include various components of a rolling element bearing, and predict the vibration response of bearings, bearing–pedestal and rotor–bearing systems, due to the presence of localised and extended bearing defects. The localised defects not only include point spalls [53, 56, 57, 59, 61, 62] (as was inadvertently the case for the impulse-train models [43–46]), but also circular spalls [60, 64], elliptical spalls (ellipsoids) [66] (as a function of Hertzian contact deformation), and line (rectangular) spalls [54, 55, 58, 63, 65, 67–69] (as a function of width and depth). The multi-body models simplify the bearing systems as lumped mass-spring-damper systems. They neglect the bending deformation of the outer and inner rings [53–65, 68, 69], except in references [66, 67], and model the rolling element-to-raceway contacts as nonlinear springs. The majority of the models that consider displacements in the radial plane were 2-D [53–58, 60, 62–64, 66–69]; however, some also consider displacements in the axial plane [59, 61, 65]. While the rolling elements were excluded in many models [53–56, 58–60, 62–64, 67], they were included in a few models [57, 61, 65, 66] as point masses; however, their inertial and centrifugal effects were mostly ignored [57, 61]. The slippage of the rolling elements was only considered by a few authors [58, 65, 66, 68, 69] in order to gain close resemblance with a typical vibration response measured in practice, and ignored by the rest. While localised damping at the contact interfaces between the rolling elements and raceways was included in a few models [56, 57, 59, 68, 69], global (structural) damping [53–55, 58, 61–67] was included in majority of the models by grounding a linear viscous damper to either the inner raceway (shaft) [61–64] or outer raceway (pedestal) [53–55, 58, 63]. All the models predicted the time domain vibration response of the outer ring/housing and inner ring [53–60, 62–69]; however, one model predicted the time domain displacement of the rolling elements [61].

The main emphasis of the multi-body models was to demonstrate the generation of vibration time-traces, and subsequently perform an envelope analysis [211, 212] on the simulated signals to primarily predict the defect-related frequency components and corresponding sidebands for model validation purposes. The problem of amplitude-mismatch between modelled and measured vibration frequencies observed in the impulse-train models [44, 46] was also reported by the authors of the multi-body models [56, 57, 62–64]. While in some cases, the predicted amplitudes have simply been corrected based on experimental results without providing an explanation [56, 57], some did not compare the modelling results with experimental measurements [53–55, 59–61, 66]; they instead compared the results with previous studies in the literature.

Explicit dynamic FE models. Explicit dynamic FE modelling of rolling element bearings, using a commercial FE software package, LS-DYNA [298], has been presented by five authors [72–76]. One of the advantages of using such a code is that one can minimise the number of assumptions that are generally considered in analytical methods. For example, the outer and inner rings, and rolling elements can be modelled as flexible bodies, the inertial and centrifugal effects of the rolling elements can be modelled, the dynamic contact interaction between the rolling elements and raceways can be studied, and above all, the interaction of defective and non-defective bearing components can be investigated. However, the majority of the FE models [72–75], except the model presented in reference [76], did not fully exploit the benefits of the explicit FE methods. The performance of the models [72–75] was compromised because either the whole outer ring of the bearing [73] or its outer surface [74] was modelled as rigid. The material behaviour, rigid or flexible, of the bearing components was not mentioned in references [72, 75]. In contrast, all the components of a bearing, such as outer and inner rings, rolling elements and cage, were modelled as flexible bodies in reference [76]; thereby, representing more accurate bearing stiffness and consequently the vibration response.

Unrealistically high instantaneous acceleration levels of magnitudes 10^7 g, 4,000 g, and 15,000 g were reported in references [73], [74], and [75], respectively, whereas realistic levels of 180 g were shown in reference [76]. While no experimental results were shown in references [72, 73], the measured acceleration levels were shown as 100 g and 10 g in references [74] and [75] compared to the simulated levels of 4,000 g and 15,000 g, respectively. A favourable comparison between the modelled and measured vibration response of a rolling element bearing was reported in reference [76]. Furthermore, the numerically modelled results were low-pass filtered with a cut-off frequency of either 500 Hz or 800 Hz resulting in the elimination of all high-frequency characteristics of the defect-related impulses [74]. As the FE modelling results were not validated against the experimental results due to the significant mismatch between their acceleration levels [74, 75], they were validated on the basis of the comparison of their predicted frequency components with those of the basic bearing kinematic frequencies. The work presented in reference [76] not only provided an experimental verification of the FE simulated vibration response, but also reported on the favourable agreement of the FE simulated and analytically estimated rolling element-to-raceway contact forces [79].

Dynamic interaction of the rolling elements with raceways (rolling element-to-raceway contact forces) was only presented in reference [76] and ignored by the rest who presented explicit FE [72–75] and multi-body models [53–67]. An in-depth analysis of the contact forces and their correlation with the bearing vibration signals led to an explanation of the physical mechanism by which defect-related impulsive forces, and consequently vibrations, are generated in defective rolling element bearings [76]. It has also been highlighted that a much higher acceleration signal is generated when a rolling element re-stresses between the raceways compared to when it strikes a defective raceway surface within a bearing [76].

Defect-related vibration characteristics. It was found that a defect-related transient vibration signal is composed of two parts/events [76, 79, 120, 121, 124]; 1) the entry of rolling elements into a defect, and 2) the exit of the rolling elements out of the defect. While the entry-related event was considered to be a low-frequency event with no indication of impulse-like characteristics [76, 79, 120, 121, 124], the exit-related event was considered to be a high-frequency event that is responsible for generating a burst of multiple, short-duration, impulses [76–79]. These impulses, which are generally observed in practice in measured bearing acceleration signals, excite a broad range of frequencies that can cause the ringing of bearing resonant modes. The energy distribution of the modelled vibration signatures associated with the entry- and exit-related events was highlighted on a spectrogram plot (time–frequency diagram) [79]. With the aim of estimating the average size of a defect, a few authors have proposed algorithms (signal processing techniques) to enhance the separation of the entry- and exit-related vibration signatures [67, 124], whereas some [76, 79, 120, 121] used the time-separation between the distinct signatures.

7. Future research directions

A number of authors have contributed significantly to a variety of aspects related to rolling element bearings since the late 1800s [153]. These aspects broadly range from understanding the onset of subsurface fatigue cracks and their subsequent growth to surface spalls [4, 5, 129–132], to the development of bearing life prediction models [154–191], to understanding the science of bearing materials for enhancing the material quality [139–149] in order to increase bearing life. The kinematics and dynamics [133, 326–341] of rolling element bearings have been understood, and several commercial codes and software packages are available to solve the dynamics of rolling element bearings — ADORE (Advanced Dynamics of Rolling Elements) [342], COBRA (Computer Optimized Ball and Roller Bearing Analysis) [343], BEAST (Bearing Simulation Tool) [344], and IBDAS (Integrated Bearing Dynamic Analysis System) [345]. The vibration response for non-defective [19–42] and defective rolling element bearings [43–119] along with the diagnosis of rolling element bearing faults [3, 6–18] have also been well documented in the literature. Despite a wealth of literature, a few research directions are discussed in the concluding paragraphs to be followed.

To investigate the effects on the vibration characteristics of defective rolling element bearings, a full parametric study could be conducted that could include a matrix of parameters, which can be varied. These parameters may include load (both radial and axial) on a bearing, rotational speed, clearance within a bearing, and various defect types. The types of bearing defects may range from line, to area, to extended area spalls having different profiles of surface roughness, which can be made similar to operational defects observed in real-world applications. The location of raceway spalls could also be varied in and out of the bearing load zone so that differences between the vibration responses could be studied.

In addition to investigating the vibration response of defective bearings, acoustic radiation from the bearings should also be studied. An interesting area where noise from rolling element bearings is primarily used for their diagnosis is the railway industry [79]. Bearing acoustic monitors [346], initially tested in the 1980s [347–350], are commonly used these days in the industry to detect defective bearings of a travelling train using the acquired noise signals [351–354].

Understanding the vibro-acoustic characteristics of various defect types would not only improve the diagnosis of defective bearings but also result in a reliable prognosis of the defects. This would result in estimating the remaining useful life of a bearing, eventually saving significant operational and maintenance costs.

Acknowledgments

This work was conducted as a part of ARC Linkage funded project LP110100529.

Appendix A. Bearing Defect Frequencies

For the case of a stationary outer ring and rotating inner ring, following are the characteristic defect frequencies of a rolling element bearing rotating at a frequency f_s [2, page 994]:

$$f_c = \frac{f_s}{2}\left(1 - \frac{D_r}{D_p}\cos\alpha\right) \tag{A.1}$$

$$f_{\text{bpo}} = \frac{f_s \times N_r}{2}\left(1 - \frac{D_r}{D_p}\cos\alpha\right) \tag{A.2}$$

$$f_{\text{bpi}} = \frac{f_s \times N_r}{2}\left(1 + \frac{D_r}{D_p}\cos\alpha\right) \tag{A.3}$$

$$f_{\text{bs}} = \frac{f_s \times D_p}{2 \times D_r}\left[1 - \left(\frac{D_r}{D_p}\cos\alpha\right)^2\right] \tag{A.4}$$

$f_{\mathbf{c}}$ cage frequency, commonly referred to as fundamental train frequency — it is the rotational speed of the cage in a rolling element bearing,

$f_{\mathbf{bpo}}$ ball pass frequency outer raceway (BPFO), commonly referred to as outer raceway defect frequency — it is the rate at which the rolling elements pass a point on the outer raceway within a rolling element bearing,

$f_{\mathbf{bpi}}$ ball pass frequency inner raceway (BPFI), commonly referred to as inner raceway defect frequency — it is the rate at which the rolling elements pass a point on the inner raceway within a rolling element bearing,

$f_{\mathbf{bs}}$ ball spin frequency (BSF), commonly referred to as ball or roller defect frequency — it is the rate of rotation of a rolling element about its own axis,

D_p bearing pitch diameter,

D_r rolling element diameter,

N_r number of rolling elements, and

α contact angle.

These frequencies are kinematic frequencies that are based on the geometry of a rolling element bearing. These frequencies do no take into account the slippage of the rotating components. As a result, actual characteristic defect frequencies slightly differ from those predicted using the aforementioned equations.

[1] H. T. Morton, Anti-Friction Bearings, Second Edition, Ann Arbor, MI, 1965.

[2] T. A. Harris, Rolling Bearing Analysis, Fourth Edition, John Wiley & Sons, 2001.

[3] I. Howard, A review of rolling element bearing vibration: "detection, diagnosis and prognosis", Tech. Rep. DSTO-RR-0013, Defence Science and Technology Organisation, Australia (October 1994).

[4] W. E. Littmann, The mechanism of contact fatigue, in: P. M. Ku (Ed.), Interdisciplinary approach to the lubrication of concentrated contacts, no. NASA SP-237, National Aeronautics and Space Administration, Washington, DC, 1970, pp. 309–378.

[5] W. E. Littmann, R. L. Widner, Propagation of contact fatigue from surface and subsurface origins, Journal of Basic Engineering 88 (3) (1966) 624–636. doi:10.1115/1.3645922.

[6] N. Tandon, A. Choudhury, A review of vibration and acoustic measurement methods for the detection of defects in rolling element bearings, Tribology International 32 (8) (1999) 469–480. doi:10.1016/S0301-679X(99)00077-8.

[7] D. R. Houser, M. J. Drosjack, Vibration signal analysis techniques, Tech. rep., U.S. Army Air Mobility Research and Development Laboratory (1973).
[8] R. A. Collacott, Vibration monitoring and diagnosis, Techniques for Cost-effective Plant Maintenance, Halsted Press, John Wiley & Sons, Inc., New York, 1979.
[9] L. M. Roger, The application of vibration analysis and acoustic emission source location to on-line condition monitoring of anti-friction bearings, Tribology International 12 (2) (1979) 51–58. doi:10.1016/0301-679X(79)90001-X.
[10] N. S. Swansson, S. C. Favaloro, Applications of vibration analysis to the condition monitoring of rolling element bearings, Tech. Rep. ARL-AERO-PROP-R-163, Defence Science and Technology Organisation, Australia (January 1984).
[11] A. Choudhury, N. Tandon, Application of acoustic emission technique for the detection of defects in rolling element bearings, Tribology International 33 (1) (2000) 39–45. doi:10.1016/S0301-679X(00)00012-8.
[12] J. Antoni, The spectral kurtosis: A useful tool for characterising non-stationary signals, Mechanical Systems and Signal Processing 20 (2) (2006) 282–307. doi:10.1016/j.ymssp.2004.09.001.
[13] J. Antoni, R. B. Randall, The spectral kurtosis: Application to the vibratory surveillance and diagnostics of rotating machines, Mechanical Systems and Signal Processing 20 (2) (2006) 308–331. doi:10.1016/j.ymssp.2004.09.002.
[14] J. Antoni, Fast detection of the kurtogram for the detection of transient faults, Mechanical Systems and Signal Processing 21 (1) (2007) 108–124. doi:10.1016/j.ymssp.2005.12.002.
[15] D. Mba, B. K. N. Rao, Development of acoustic emission technology for condition monitoring and diagnosis of rotating machines; bearings, pumps, gearboxes, engines and rotating structures, The Shock and Vibration Digest 38 (1) (2006) 3–16. doi:10.1177/0583102405059054.
[16] A. K. S. Jardine, D. Lin, D. Banjevic, A review on machinery diagnostics and prognostics implementing condition-based maintenance, Mechanical Systems and Signal Processing 20 (7) (2006) 1483–1510. doi:10.1016/j.ymssp.2005.09.012.
[17] R. B. Randall, J. Antoni, Rolling element bearing diagnostics — A tutorial, Mechanical Systems and Signal Processing 25 (2) (2011) 485–520. doi:10.1016/j.ymssp.2010.07.017.
[18] R. B. Randall, Vibration-based condition monitoring, First Edition, Industrial, aerospace, and automotive applications, John Wiley & Sons, Ltd, 2011.
[19] H. Perret, Elastische Spielschwingungen konstant belasteter Wälzlager, Werkstatt und Betrieb 83 (8) (1950) 354–358.
[20] H. Perret, Die Lagerluft als Bestimmungsgrösse fur die Beanspruchungeines Wälzlagers, Werkstatt und Betrieb 83 (4) (1950) 131–134.
[21] H. Perret, Schwingungen in Wälzlagern bei statisch bestimmter Abstützung, VDI-Forschungs (434) (1952) 17–28.
[22] H. Perret, Wälzlager als Schwingungserreger, Werkstattstechnik und Maschinenbau 40 (1) (1950) 5–9.
[23] E. Meldau, Die Bewegung der Achse von Wälzlagern bei geringen Drehzahlen, Werkstatt und Betrieb 84 (7) (1951) 308–313.
[24] E. Meldau, Werkstatt und Betrieb 84 (4) (1951) 143.
[25] E. Meldau, Werkstatt und Betrieb 85 (2) (1952) 56.
[26] E. Meldau, Konstruktion 4 (3) (1952) 79.
[27] T. E. Tallian, O. G. Gustafsson, The mechanics of rolling-element bearing vibrations, Transactions of the American Society of Mechanical Engineers Paper No. 58-A-292.
[28] A. Tamura, O. Taniguchi, Ball bearing vibrations: 1st Report, On the radial vibration caused by passing balls, Transactions of The Japan Society of Mechanical Engineers 26 (161) (1960) 19–25. doi:10.1299/kikai1938.26.19.
[29] A. Tamura, O. Taniguchi, Ball bearing vibrations: 2nd Report, On the subharmonic vibration of order 1/2 caused by passing balls, Transactions of The Japan Society of Mechanical Engineers 26 (167) (1960) 877–883. doi:10.1299/kikai1938.26.877.
[30] A. Tamura, O. Taniguchi, Ball bearing vibrations: 3rd Report, On the axial vibration caused by passing balls, Transactions of The Japan Society of Mechanical Engineers 26 (170) (1960) 1428–1434. doi:10.1299/kikai1938.26.1428.
[31] A. Tamura, O. Taniguchi, Ball bearing vibrations: 4th Report, On the nonlinear vibrations in axial direction, Transactions of The Japan Society of Mechanical Engineers 27 (179) (1961) 1146–1153. doi:10.1299/kikai1938.27.1146.
[32] A. Tamura, O. Taniguchi, Ball bearing vibrations: 5th Report, On the device to reduce the vibration caused by a ball bearing, Transactions of The Japan Society of Mechanical Engineers 27 (182) (1962) 1505–1509. doi:10.1299/kikai1938.27.1509.
[33] A. Tamura, O. Taniguchi, Ball bearing vibrations: 6th Report, On the vibration of a ball bearing under light load, Transactions of The Japan Society of Mechanical Engineers 28 (188) (1962) 492–499. doi:10.1299/kikai1938.28.492.
[34] H. Tamura, Y. Tsuda, On the spring characteristics of a ball bearing: extreme characteristics with many balls, Bulletin of The Japan Society of Mechanical Engineers 23 (180) (1980) 961–969. doi:10.1299/jsme1958.23.961.
[35] H. Tamura, Y. Tsuda, On the spring characteristics of a ball bearing: fluctuation due to ball revolution, Bulletin of The Japan Society of Mechanical Engineers 23 (185) (1980) 1905–1912. doi:10.1299/jsme1958.23.1905.
[36] H. Tamura, E. H. Gad, T. Kondou, Y. Tsuda, A. Sueoka, The static running accuracy of ball bearings, Memoirs of the Faculty of Engineering 43 (4) (1983) 285–316.
[37] E. H. Gad, T. Kondou, H. Tamura, Spring property of ball bearing, Memoirs of the Faculty of Engineering 43 (3) (1983) 243–264.
[38] E. H. Gad, S. Fukata, H. Tamura, Computer simulation of rotor radial vibrations due to ball bearings, Memoirs of the Faculty of Engineering 44 (1) (1984) 83–111.
[39] E. H. Gad, S. Fukata, H. Tamura, Computer simulation of rotor axial and radial vibrations based on ball bearings, Memoirs of the Faculty of Engineering 44 (2) (1984) 169–183.
[40] S. Fukata, E. H. Gad, T. Kondou, T. Ayabe, H. Tamura, On the radial vibration of ball bearings: computer simulation, Bulletin of The Japan Society of Mechanical Engineers 28 (239) (1985) 899–904. doi:10.1299/jsme1958.28.899.

[41] H. Tamura, E. H. Gad, T. Kondou, T. Ayabe, A. Sueoka, On the static running accuracy of ball bearings, Bulletin of The Japan Society of Mechanical Engineers 28 (240) (1985) 1240–1246. doi:10.1299/jsme1958.28.1240.
[42] S. H. Ghafari, E. M. Rahman, F. Golnaraghi, F. Ismail, Vibrations of balanced fault-free ball bearings, Journal of Sound and Vibration 329 (9) (2010) 1332–1347. doi:10.1016/j.jsv.2009.11.003.
[43] P. D. McFadden, J. D. Smith, Model for the vibration produced by a single point defect in a rolling element bearing, Journal of Sound and Vibration 96 (1) (1984) 69–82. doi:10.1016/0022-460X(84)90595-9.
[44] P. D. McFadden, J. D. Smith, The vibration produced by multiple point defects in a rolling element bearing, Journal of Sound and Vibration 98 (2) (1985) 263–273. doi:10.1016/0022-460X(85)90390-6.
[45] Y. T. Su, S. J. Lin, On initial fault detection of a tapered roller bearing: Frequency domain analysis, Journal of Sound and Vibration 155 (1) (1992) 75–84. doi:10.1016/0022-460X(92)90646-F.
[46] N. Tandon, A. Choudhury, An analytical model for the prediction of the vibration response of rolling element bearings due to a localized defect, Journal of Sound and Vibration 205 (3) (1997) 275–292. doi:10.1006/jsvi.1997.1031.
[47] D. Brie, Modelling of the spalled rolling element bearing vibration signal: An overview and some new results, Mechanical Systems and Signal Processing 14 (3) (2000) 353–369. doi:10.1006/mssp.1999.1237.
[48] D. Ho, R. B. Randall, Optimisation of bearing diagnostics techniques using simulated and actual bearing fault signals, Mechanical Systems and Signal Processing 14 (5) (2000) 763–788. doi:10.1006/mssp.2000.1304.
[49] R. B. Randall, J. Antoni, S. Chobsaard, The relationship between spectral correlation and envelope analysis in the diagnostics of bearing faults and other cyclostationary machine signals, Mechanical Systems and Signal Processing 15 (5) (2001) 945–962. doi:10.1006/mssp.2001.1415.
[50] J. Antoni, R. B. Randall, Differential diagnosis of gear and bearing faults, Journal of Vibration and Acoustics 124 (2) (2002) 165–171. doi:10.1115/1.1456906.
[51] J. Antoni, R. B. Randall, A stochastic model for simulation and diagnostics of rolling element bearings with localized faults, Journal of Vibration and Acoustics 125 (3) (2003) 282–289. doi:10.1115/1.1569940.
[52] M. Behzad, A. R. Bastami, D. Mba, A new model for estimating vibrations generated in the defective rolling element bearings, Journal of Vibration and Acoustics 133 (4) (2011) 041011 (8 pages). doi:10.1115/1.4003595.
[53] N. S. Feng, E. J. Hahn, R. B. Randall, Using transient analysis software to simulate vibration signals due to rolling element bearing defects, in: Proceedings of the Third Australian Congress on Applied Mechanics, Sydney, 2002, pp. 689–694.
[54] J. Sopanen, A. Mikkola, Dynamic model of a deep-groove ball bearing including localized and distributed defects. Part 1: Theory, Proceedings of the Institution of Mechanical Engineers, Part K: Journal of Multi-body Dynamics 217 (3) (2003) 201–211. doi:10.1243/14644190360713551.
[55] J. Sopanen, A. Mikkola, Dynamic model of a deep-groove ball bearing including localized and distributed defects. Part 2: Implementation and results, Proceedings of the Institution of Mechanical Engineers, Part K: Journal of Multi-body Dynamics 217 (3) (2003) 213–233. doi:10.1243/14644190360713560.
[56] A. Choudhury, N. Tandon, Vibration response of rolling element bearings in a rotor bearing system to a local defect under radial load, Journal of Tribology 128 (2) (2006) 252–261. doi:10.1115/1.2164467.
[57] S. Sassi, B. Badri, M. Thomas, A numerical model to predict damaged bearing vibrations, Journal of Vibration and Control 13 (11) (2007) 1603–1628. doi:10.1177/1077546307080040.
[58] N. Sawalhi, R. B. Randall, Simulating gear and bearing interactions in the presence of faults. Part I: The combined gear bearing dynamic model and the simulation of localised bearing faults, Mechanical Systems and Signal Processing 22 (8) (2008) 1924–1951. doi:10.1016/j.ymssp.2007.12.001.
[59] M. Cao, J. Xiao, A comprehensive dynamic model of double-row spherical roller bearing — Model development and case studies on surface defects, preloads, and radial clearance, Mechanical Systems and Signal Processing 22 (2) (2008) 467–489. doi:10.1016/j.ymssp.2007.07.007.
[60] A. Ashtekar, F. Sadeghi, L.-E. Stacke, A new approach to modeling surface defects in bearing dynamics simulations, Journal of Tribology 130 (4) (2008) 041103 (8 pages). doi:10.1115/1.2959106.
[61] H. Arslan, N. Aktürk, An investigation of rolling element vibrations caused by local defects, Journal of Tribology 130 (4) (2008) 041101 (12 pages). doi:10.1115/1.2958070.
[62] A. Rafsanjani, S. Abbasion, A. Farshidianfar, H. Moeenfard, Nonlinear dynamic modeling of surface defects in rolling element bearing systems, Journal of Sound and Vibration 319 (3–5a) (2009) 1150–1174. doi:10.1016/j.jsv.2008.06.043.
[63] V. N. Patel, N. Tandon, R. K. Pandey, A dynamic model for vibration studies of deep groove ball bearings considering single and multiple defects in races, Journal of Tribology 132 (4) (2010) 041101 (10 pages). doi:10.1115/1.4002333.
[64] M. S. Patil, J. Mathew, P. K. Rajendrakumar, S. Desai, A theoretical model to predict the effect of localized defect on vibrations associated with ball bearing, International Journal of Mechanical Sciences 52 (9) (2010) 1193–1201. doi:10.1016/j.ijmecsci.2010.05.005.
[65] M. Nakhaeinejad, M. D. Bryant, Dynamic modeling of rolling element bearings with surface contact defects using bond graphs, Journal of Tribology 133 (1) (2011) 011102 (12 pages). doi:10.1115/1.4003088.
[66] M. Tadina, M. Boltežar, Improved model of a ball bearing for the simulation of vibration signals due to faults during run-up, Journal of Sound and Vibration 330 (17) (2011) 4287–4301. doi:10.1016/j.jsv.2011.03.031.
[67] S. Zhao, L. Liang, G. Xu, J. Wang, W. Zhang, Quantitative diagnosis of a spall-like fault of a rolling element bearing by empirical mode decomposition and the approximate entropy method, Mechanical Systems and Signal Processing 40 (1) (2013) 154–177. doi:10.1016/j.ymssp.2013.04.006.
[68] D. Petersen, C. Howard, N. Sawalhi, A. Ahmadi, S. Singh, Analysis of bearing stiffness variations, contact forces and vibrations in radially loaded double row ball bearings with raceway defects, Mechanical Systems and Signal Processing 50–51 (2014) 139–160. doi:10.1016/j.ymssp.2014.04.014.

[69] A. Moazenahmadi, D. Petersen, C. Howard, A nonlinear dynamic vibration model of defective bearings — the importance of modelling the finite size of rolling elements, Mechanical Systems and Signal Processing Accepted for publication. doi:10.1016/j.ymssp.2014.06.006.
[70] Z. Kiral, H. Karagülle, Simulation and analysis of vibration signals generated by rolling element bearing with defects, Tribology International 36 (9) (2003) 667–678. doi:10.1016/S0301-679X(03)00010-0.
[71] Z. Kiral, H. Karagülle, Vibration analysis of rolling element bearings with various defects under the action of an unbalanced force, Mechanical Systems and Signal Processing 20 (8) (2006) 1967–1991. doi:10.1016/j.ymssp.2005.05.001.
[72] Y. Shao, W. Tu, F. Gu, A simulation study of defects in a rolling element bearing using FEA, in: International Conference on Control, Automation and Systems, Gyeonggi-do, Korea, 2010, pp. 596–599.
[73] L. Guochao, P. Wei, L. Yongcai, G. Lixin, J. Zhang, Simulation and dynamic analysis of outer ring fault on rolling bearings using explicit finite element method, China Mechanical Engineering 23 (23) (2012) 2825–2829. doi:10.3969/j.issn.1004-132X.2012.23.011.
[74] J. Liu, Y. Shao, M. J. Zuo, The effects of the shape of localized defect in ball bearings on the vibration waveform, Proceedings of the Institution of Mechanical Engineers, Part K: Journal of Multi-body Dynamics 227 (3) (2013) 261–274. doi:10.1177/1464419313486102.
[75] A. Utpat, Vibration signature analysis of defective deep groove ball bearings by numerical and experimental approach, International Journal of Scientific and Engineering Research 4 (6) (2013) 592–598.
[76] S. Singh, U. Köpke, C. Howard, D. Petersen, Analyses of contact forces and vibration response for a defective rolling element bearing using an explicit dynamics finite element model, Journal of Sound and Vibration 333 (21) (2014) 5356–5377. doi:10.1016/j.jsv.2014.05.011.
[77] S. Singh, U. Köpke, C. Howard, D. Petersen, D. Rennison, Impact generating mechanisms in damaged rolling element bearings, in: Proceedings of Acoustics, Australian Acoustical Society, Paper number 106, Victor Harbor, South Australia, Australia, 2013.
[78] S. Singh, C. Howard, C. Hansen, U. Köpke, Numerical noise generation in modelled bearing vibration signals, in: 43$^{\mathrm{rd}}$ International Congress on Noise Control Engineering, Paper number 180, Melbourne, Victoria, Australia, 2014, Accepted for publication.
[79] S. Singh, Explicit dynamics finite element modelling of defective rolling element bearings, Ph.D. thesis, School of Mechanical Engineering, The University of Adelaide, South Australia 5005 Australia (2014).
[80] N. Sawalhi, R. B. Randall, Simulating gear and bearing interactions in the presence of faults. Part II: Simulation of the vibrations produced by extended bearing faults, Mechanical Systems and Signal Processing 22 (8) (2008) 1952–1966. doi:10.1016/j.ymssp.2007.12.002.
[81] J. I. McCool, O. G. Gustafsson, Relative axis motion induced by variable elastic compliance in ball bearings, Tech. Rep. L60L023, SKF Industries, Inc., U.S. Navy Contract No. NObs-78552 (October 1960).
[82] O. G. Gustafsson, Harmonic analysis of the relative axis motion induced by variable elastic compliance in ball bearings, Tech. Rep. AL61L009, SKF Industries, Inc., U.S. Navy Contract No. NObs-78552 (March 1961).
[83] R. L. Huston, A study of elastic vibrations of the outer race of a rolling element bearing, Tech. Rep. AL61L027, SKF Industries, Inc., U.S. Navy Contract No. NObs-78552 (August 1961).
[84] O. G. Gustafsson, Analytical study of the vibration of a bearing with flexurally rigid races, Tech. Rep. AL61L032, SKF Industries, Inc., U.S. Navy Contract No. NObs-78552 (October 1961).
[85] J. I. McCool, Flexural vibrations of a ball bearing outer ring due to ball loads, Tech. Rep. AL61L037, SKF Industries, Inc., U.S. Navy Contract No. NObs-78552 (December 1961).
[86] O. G. Gustafsson, Analytical study of the radial, axial and angular vibration of a bearing with flexurally rigid races, Tech. Rep. AL62L005, SKF Industries, Inc., U.S. Navy Contract No. NObs-78552 (April 1962).
[87] O. G. Gustafsson, T. E. Tallian, Detection of damage in assembled rolling element bearings, Transactions of the American Society of Lubrication Engineers 5 (1) (1962) 197–209. doi:10.1080/05698196208972466.
[88] O. G. Gustafsson, T. E. Tallian, Final report on study of the vibration characteristics of bearings, Tech. Rep. AL69LO23, SKF Industries, Inc, U.S. Navy Contract No. NObs-78552 (December 1963).
[89] T. E. Tallian, O. G. Gustafsson, Progress in rolling bearing vibration research and control, Transactions of the American Society of Lubrication Engineers 8 (3) (1965) 195–207. doi:10.1080/05698196508972094.
[90] E. Yhland, Waviness measurement — an instrument for quality control in rolling bearing industry, in: Proceedings of the Institution of Mechanical Engineers, Conference Proceedings, Vol. 182, 1967, pp. 438–445. doi:10.1243/PIME_CONF_1967_182_341_02.
[91] L. E. Lura, R. B. Walker, Bearing noise reduction, Society of Automotive Engineers SAE Technical Paper 720733. doi:10.4271/720733.
[92] C. S. Sunnersjö, Rolling bearing vibrations — the effects of varying compliance, manufacturing tolerances and wear, Ph.D. thesis, University of Aston (1976).
[93] C. S. Sunnersjö, Varying compliance vibrations of rolling bearings, Journal of Sound and Vibration 58 (3) (1978) 363–373. doi:10.1016/S0022-460X(78)80044-3.
[94] C. S. Sunnersjö, Rolling bearing vibrations — the effects of geometrical imperfections and wear, Journal of Sound and Vibration 98 (4) (1985) 455–474. doi:10.1016/0022-460X(85)90256-1.
[95] Y.-T. Su, M.-H. Lin, M.-S. Lee, The effects of surface irregularities on roller bearing vibrations, Journal of Sound and Vibration 165 (3) (1993) 455–466. doi:10.1006/jsvi.1993.1270.
[96] L. D. Meyer, B. Weichbrodt, F. F. Ahlgren, An analytical model for ball bearing vibrations to predict vibration response to distributed defects, Journal of Mechanical Design 102 (2) (1980) 205–210. doi:10.1115/1.3254731.
[97] F. P. Wardle, Vibration forces produced by waviness of the rolling surfaces of thrust loaded ball bearings, Part 1: Theory,

Proceedings of the Institution of Mechanical Engineers, Part C: Journal of Mechanical Engineering Science 202 (5) (1988) 305–312. doi:10.1243/PIME_PROC_1988_202_127_02.

[98] F. P. Wardle, Vibration forces produced by waviness of the rolling surfaces of thrust loaded ball bearings, Part 2: Experimental validation, Proceedings of the Institution of Mechanical Engineers, Part C: Journal of Mechanical Engineering Science 202 (5) (1988) 313–319. doi:10.1243/PIME_PROC_1988_202_128_02.

[99] E. Yhland, A linear theory of vibrations caused by ball bearings with form errors operating at moderate speed, Journal of Tribology 114 (2) (1992) 348–359. doi:10.1115/1.2920894.

[100] N. Aktürk, M. Uneeb, R. Gohar, The effect of number of ball and preloads on vibrations associated with ball bearings, Journal of Tribology 119 (4) (1997) 747–753. doi:10.1115/1.2833880.

[101] A. Choudhury, N. Tandon, A theoretical model to predict vibration response of rolling bearings to distributed defects under radial load, Journal of Vibration and Acoustics 120 (1) (1998) 214–220. doi:10.1115/1.2893808.

[102] K. Ono, Y. Okada, Analysis of ball bearing vibrations caused by outer race waviness, Journal of Vibration and Acoustics 120 (4) (1998) 901–908. doi:10.1115/1.2893918.

[103] N. Aktürk, The effect of waviness on vibrations associated with ball bearings, Journal of Tribology 121 (4) (1999) 667–677. doi:10.1115/1.2834121.

[104] N. Tandon, A. Choudhury, A theoretical model to predict the vibration response of rolling bearings in a rotor bearing system to distributed defects under radial load, Journal of Tribology 122 (3) (2000) 609–615. doi:10.1115/1.555409.

[105] M. Tiwari, K. Gupta, O. Prakash, Effect of radial internal clerance of a ball bearing on the dynamics of a balanced horizontal rotor, Journal of Sound and Vibration 238 (5) (2000) 723–756. doi:10.1006/jsvi.1999.3109.

[106] M. Tiwari, K. Gupta, O. Prakash, Dynamic response of an unbalanced rotor supported on ball bearings, Journal of Sound and Vibration 238 (5) (2000) 757–779. doi:10.1006/jsvi.1999.3108.

[107] G. Jang, S. W. Jeong, Nonlinear excitation model of ball bearing waviness in a rigid rotor supported by two or more ball bearings considering five degrees of freedom, Journal of Tribology 124 (1) (2001) 82–90. doi:10.1115/1.1398289.

[108] S. P. Harsha, K. Sandeep, R. Prakash, Non-linear dynamic behaviors of rolling element bearings due to surface waviness, Journal of Sound and Vibration 272 (3–5) (2004) 557–580. doi:10.1016/S0022-460X(03)00384-5.

[109] S. P. Harsha, P. K. Kankar, Stability analysis of rotor bearing system due to surface waviness and number of balls, International Journal of Mechanical Sciences 46 (7) (2004) 1057–1081. doi:10.1016/j.ijmecsci.2004.07.007.

[110] S. P. Harsha, The effect of ball size variations on nonlinear vibration associated with ball bearings, Proceedings of the Institution of Mechanical Engineers, Part K: Journal of Multi-body Dynamics 218 (4) (2004) 191–200. doi:10.1243/1464419043541455.

[111] G. Jang, S. W. Jeong, Vibration analysis of a rotating system due to the effect of ball bearing waviness, Journal of Sound and Vibration 269 (3–5) (2004) 709–726. doi:10.1016/S0022-460X(03)00127-5.

[112] B. Changqing, X. Qingyu, Dynamic model of ball bearings with internal clearance and waviness, Journal of Sound and Vibration 294 (1–2) (2006) 23–48. doi:10.1016/j.jsv.2005.10.005.

[113] S. P. Harsha, C. Nataraj, P. K. Kankar, The effect of ball waviness on nonlinear vibration associated with rolling element bearings, International Journal of Acoustics and Vibration 11 (2) (2006) 56–66.

[114] S. P. Harsha, Nonlinear dynamic analysis of rolling element bearings due to cage run-out and number of balls, Journal of Sound and Vibration 289 (1–2) (2006) 360–381. doi:10.1016/j.jsv.2005.02.021.

[115] S. P. Harsha, Rolling bearing vibrations — the effect of surface waviness and radial internal clearance, International Journal of Computational Methods in Engineering Science and Mechanics 7 (2) (2006) 91–111. doi:10.1080/155022891010015.

[116] S. H. Upadhyay, S. C. Jain, S. P. Harsha, Non-linear vibration signature analysis of high-speed rotating shaft due to ball size variations and varying number of balls, Proceedings of the Institution of Mechanical Engineers, Part K: Journal of Multi-body Dynamics 223 (2) (2009) 83–105. doi:10.1243/14644193JMBD187.

[117] S. H. Upadhyay, S. P. Harsha, S. C. Jain, Vibration signature analysis of high speed unbalanced rotors supported by rolling element bearings due to off-sized rolling elements, International Journal of Acoustics and Vibration 14 (3) (2009) 163–171.

[118] C. K. Babu, N. Tandon, R. K. Pandey, Vibration modeling of a rigid rotor supported on the lubricated angular contact ball bearings considering six degrees of freedom and waviness on balls and races, Journal of Vibration and Acoustics 134 (1) (2012) 011006 (12 pages). doi:10.1115/1.4005140.

[119] P. K. Kankar, S. C. Sharma, Nonlinear vibration signature analysis of a high speed rotor bearing system due to race imperfection, Journal of Computational and Nonlinear Dynamics 7 (1) (2012) 011014 (16 pages). doi:10.1115/1.4004962.

[120] I. K. Epps, An investigation into vibrations excited by discrete faults in rolling element bearings, Ph.D. thesis, School of Mechanical Engineering, The University of Canterbury, Christchurch, New Zealand (1991).

[121] I. K. Epps, H. McCallion, An investigation into the characteristics of vibration excited by discrete faults in rolling element bearings, in: Fourth Annual Vibration Association of New Zealand Conference, Christchurch, New Zealand, 1993.

[122] P. Berret, J. M. Laskey, Small portable analyzer diagnostic equipment (spade) program — diagnostic software validation, Tech. rep., RCA Automated Systems Division, Burlington, MA., United States. Army Aviation Systems Command (July 1984).

[123] M. J. Dowling, Application of non-stationary analysis to machinery monitoring, in: Proceedings of IEEE International Conference on Acoustics, Speech, and Signal Processing, Vol. 1, 1993, pp. 59–62. doi:10.1109/ICASSP.1993.319054.

[124] N. Sawalhi, R. B. Randall, Vibration response of spalled rolling element bearings: Observations, simulations and signal processing techniques to track the spall size, Mechanical Systems and Signal Processing 25 (3) (2011) 846–870. doi:10.1016/j.ymssp.2010.09.009.

[125] D. Petersen, C. Howard, Z. Prime, Varying stiffness and load distributions in defective ball bearings: analytical formulation and application to defect size estimation, Journal of Sound and Vibration 337 (2015) 284–300.

doi:10.1016/j.jsv.2014.10.004.
[126] ASM Handbook Volume 19: Fatigue and Fracture, Vol. 19 of ASM Handbook, ASM International, 1996.
[127] F. Ellyin, Fatigue Damage, Crack Growth and Life Prediction, Springer, 1997.
[128] S. Suresh, Fatigue of materials, Cambridge University Press, Cambridge, UK, 1998.
[129] T. E. Tallian, Failure Atlas for Hertz Contact Machine Elements, ASME Press, New York, 1992.
[130] A. V. Olver, The mechanism of rolling contact fatigue: An update, Proceedings of the Institution of Mechanical Engineers, Part J: Journal of Engineering Tribology 219 (5) (2005) 313–330. doi:10.1243/135065005X9808.
[131] J. Halme, P. Andersson, Rolling contact fatigue and wear fundamentals for rolling bearing diagnostics — state of the art, Proceedings of the Institution of Mechanical Engineers, Part J: Journal of Engineering Tribology 224 (4) (2009) 377–393. doi:10.1243/13506501JET656.
[132] F. Sadeghi, N. K. Arakere, B. Jalalahmadi, T. S. Slack, N. Raje, A review of rolling contact fatigue, Journal of Tribology 131 (4) (2009) 041403 (15 pages). doi:10.1115/1.3209132.
[133] T. A. Harris, M. N. Kotzalas, Essential Concepts of Bearing Technology, CRC Press, Taylor & Francis Group, 2007.
[134] H. Hertz, Über die Berührung fester elastischer Körper (on the contact of elastic solids). Reprinted in English Miscellaneous Papers by H. Hertz, Eds. Jones and Schott, London: Macmillan, 1896. [90, 243], Journal of Reine and Angewandte Mathematik 92 (1882) 156–171.
[135] H. Hertz, Über die Berührung fester elastischer Körper and über die Harte(on the contact of rigid elastic solids and on hardness). Reprinted in English Miscellaneous Papers by H. Hertz, Eds. Jones and Schott, London: Macmillan, 1896. [90, 156], Verhandlungen des Vereins zur Beförderung des Gewerbefleisses.
[136] K. L. Johnson, Contact Mechanics, First Edition, Press Syndicate of the University of Cambridge, 1985.
[137] A. Palmgren, Die lebensdauer von kugellagern (the service life of ball bearings), Zeitschrift des Vereines Deutscher Ingenieure 68 (14) (1924) 339–341, NASA Technical Translation (NASA TT F-13460).
[138] A. Palmgren, Ball and roller bearing engineering, SKF Industries, Philadelphia, PA, 1945.
[139] J. A. Martin, S. F. Borgese, A. D. Eberhardt, Microstructural alterations of rolling-bearing steel undergoing cyclic stressing, Journal of Basic Engineering 88 (3) (1966) 555–565. doi:10.1115/1.3645902.
[140] E. N. Bamberger, Effect of materials — metallurgy viewpoint, in: P. M. Ku (Ed.), Interdisciplinary approach to the lubrication of concentrated contacts, National Aeronautics and Space Administration, Washington DC, Troy, NY, 1969, NASA Special Report, SP-237, pages 409–438.
[141] H. Swahn, P. C. Becker, O. Vingsbo, Martensite decay during rolling contact fatigue in ball bearings, Metallurgical Transactions A 7 (8) (1976) 1099–1110. doi:10.1007/BF02656592.
[142] A. P. Voskamp, R. Österlund, P. C. Becker, O. Vingsbo, Gradual changes in residual stress and microstructure during contact fatigue in ball bearings, Journal of Metals Technology 7 (1980) 14–21. doi:10.1179/030716980803286676.
[143] R. Österlund, O. Vingsbo, Phase changes in fatigued ball bearings, Metallurgical Transactions A 11 (5) (1980) 701–707. doi:10.1007/BF02661199.
[144] P. C. Becker, Microstructural changes around non-metallic inclusions caused by rolling-contact fatigue of ball bearing steels, Metals Technology 8 (10) (1981) 234–243. doi:10.1179/030716981803275415.
[145] A. P. Voskamp, Material response to rolling contact loading, Journal of Tribology 107 (3) (1985) 359–364. doi:10.1115/1.3261078.
[146] A. P. Voskamp, E. J. Mittemeijer, Crystallographic preferred orientation induced by cyclic rolling contact loading, Metallurgical and Materials Transactions A 27 (11) (1996) 3445–3465. doi:10.1007/BF02595437.
[147] A. P. Voskamp, E. J. Mittemeijer, The effect of the changing microstructure on the fatigue behavior during cyclic rolling contact loading, Zeitschrift für Metallkunde 88 (4) (1997) 310–319.
[148] A. P. Voskamp, Fatigue and material response in rolling contact, in: J. J. C. Hoo, W. B. Green (Eds.), Bearing Steels: Into the 21st Century, no. ASTM STP 1327, American Society of Testing and Materials, West Conshohocken, PA 19428-2959, 1998, pp. 152–166.
[149] A. P. Voskamp, Microstructural stability and bearing performance, in: J. M. Beswick (Ed.), Bearing Steel Technology, no. ASTM STP 1419, American Society of Testing and Materials, West Conshohocken, PA 19428-2959, 2002, pp. 443–456.
[150] Timken bearing damage analysis with lubrication reference guide, Reference guide.
URL http://www.timken.com/
[151] T. E. Tallian, On competing failure modes in rolling contact, Transactions of the American Society of Lubrication Engineers 10 (4) (1967) 418–439. doi:10.1080/05698196708972201.
[152] ISO 15243 — Rolling bearings — Damage and failures — Terms, characteristics and causes, international Organization for Standardization (2004).
[153] R. Stribeck, Reports from the central laboratory for scientific technical investigation, Transactions of the American Society of Mechanical Engineers 29 (1907) 420–466, translation by H. Hess, 1900.
[154] G. Lundberg, A. Palmgren, Dynamic capacity of rolling bearings, Acta Politechnica Mechanical Engineering Series 1 (3) (1947) 1–52, Royal Swedish Academy of Engineering Sciences.
[155] G. Lundberg, A. Palmgren, Dynamic capacity of roller bearings, Acta Politechnica Mechanical Engineering Series 2 (4) (1952) 96–127, Royal Swedish Academy of Engineering Sciences.
[156] Y. P. Chiu, T. E. Tallian, J. I. McCool, J. A. Martin, A mathematical model of spalling fatigue failure in rolling contact, Transactions of the American Society of Lubrication Engineers 12 (2) (1969) 106–116. doi:10.1080/05698196908972252.
[157] Y. P. Chiu, T. E. Tallian, J. I. McCool, An engineering model of spalling fatigue failure in rolling contact: I. The subsurface model, Wear 17 (5–6) (1971) 433–446. doi:10.1016/0043-1648(71)90049-4.
[158] T. E. Tallian, J. I. McCool, An engineering model of spalling fatigue failure in rolling contact: II. The surface model, Wear 17 (5–6) (1971) 447–461. doi:10.1016/0043-1648(71)90050-0.

[159] T. E. Tallian, An engineering model of spalling fatigue failure in rolling contact: III. Engineering discussion and illustrative examples, Wear 17 (5–6) (1971) 463–480. doi:10.1016/0043-1648(71)90051-2.
[160] T. E. Tallian, Prediction of rolling contact fatigue life in contaminated lubricant: Part I – Mathematical Model, Journal of Lubrication Technology 98 (2) (1976) 251–257. doi:10.1115/1.3452814.
[161] T. E. Tallian, Prediction of rolling contact fatigue life in contaminated lubricant: Part II – Experimental, Journal of Lubrication Technology 98 (3) (1976) 384–392. doi:10.1115/1.3452865.
[162] T. E. Tallian, A unified model for rolling contact life prediction, Journal of Lubrication Technology 104 (3) (1982) 336–346. doi:10.1115/1.3253216.
[163] R. R. Miller, L. M. Keer, H. S. Cheng, On the mechanics of fatigue crack growth due to contact loading, Proceedings of the Royal Society of London. Series A, Mathematical and Physical Sciences 397 (1813) (1985) 197–209. doi:10.1098/rspa.1985.0011.
[164] E. Ioannides, T. A. Harris, A new fatigue model for rolling bearings, Journal of Tribology 107 (3) (1985) 367–377. doi:10.1115/1.3261081.
[165] H. Schlicht, E. Schreiber, O. Zwirlein, Fatigue and failure mechanism of bearings, in: International Conference on Fatigue of Engineering Materials and Structures, Vol. 1 of Proceedings of the Institution of Mechanical Engineers, Institution of Mechanical Engineers, University of Sheffield, 1986, pp. 85–90.
[166] T. E. Tallian, Unified rolling contact life model with fatigue limit, Wear 107 (1) (1986) 13–36. doi:10.1016/0043-1648(86)90044-X.
[167] T. E. Tallian, Rolling bearing life prediction. Correction for material and operating conditions. Part I: General model and basic life, Journal of Lubrication Technology 110 (1) (1988) 2–6. doi:10.1115/1.3261570.
[168] T. E. Tallian, Rolling bearing life prediction. Correction for material and operating conditions. Part II: The correction factors, Journal of Lubrication Technology 110 (1) (1988) 7–12. doi:10.1115/1.3261579.
[169] X. Leng, Q. Cheng, E. Shao, Initiation and propagation of case crushing cracks in rolling contact fatigue, Wear 122 (1) (1988) 33–43. doi:10.1016/0043-1648(88)90004-X.
[170] ISO 281 — Rolling bearings — Dynamic load ratings and rating life, international Organization for Standardization (1989).
[171] T. E. Tallian, Simplified contact fatigue life prediction model — Part I: Review of published models, Journal of Tribology 114 (2) (1992) 207–213. doi:10.1115/1.2920875.
[172] T. E. Tallian, Simplified contact fatigue life prediction model — Part II: New model, Journal of Tribology 114 (2) (1992) 214–220. doi:10.1115/1.2920876.
[173] J. Chalsma, E. V. Zaretsky, Design for life, plan for death, Machine Design 66 (15) (1994) 57–59.
[174] T. A. Harris, J. I. McCool, On the accuracy of rolling bearing fatigue life prediction, Journal of Tribology 118 (2) (1996) 297–309. doi:10.1115/1.2831299.
[175] E. Ioannides, G. Bergling, A. Gabelli, An analytical formulation for the life of rolling bearings, Acta Polytechnica Scandinavica, Mechanical Engineering Series 137 (1999) 77, Finnish Academy of Technology, Espoo.
[176] M. N. Kotzalas, T. A. Harris, Fatigue failure progression in ball bearings, Journal of Tribology 123 (2) (2001) 238–242. doi:10.1115/1.1308013.
[177] I. I. Kudish, K. W. Burris, Modern state of experimentation and modeling in contact fatigue phenomenon: Part II — Analysis of existing statistical mathematical models of bearing and gear fatigue life. New statistical model of contact fatigue, Tribology Transactions 43 (2) (2000) 293–301. doi:10.1080/10402000008982343.
[178] S. Shimizu, Fatigue limit concept and life prediction model for rolling contact machine elements, Tribology Transactions 45 (1) (2002) 39–46. doi:10.1080/10402000208982519.
[179] M. N. Kotzalas, Statistical distribution of tapered roller bearing fatigue lives at high levels of reliability, Journal of Tribology 127 (4) (2005) 865–870. doi:10.1115/1.2000981.
[180] L. M. Keer, M. D. Bryant, A pitting model for rolling contact fatigue, Journal of Lubrication Technology 105 (2) (1983) 198–205. doi:10.1115/1.3254565.
[181] R. S. Zhou, H. S. Cheng, T. Mura, Micropitting in rolling and sliding contact under mixed lubrication, Journal of Tribology 111 (4) (1989) 605–613. doi:10.1115/1.3261984.
[182] V. Bhargava, G. T. Hahn, C. A. Rubin, Rolling contact deformation, etching effects and failure of high strength steels, Metallurgical Transactions A 21 (7) (1990) 1921–1931. doi:10.1007/BF02647240.
[183] W. Cheng, H. S. Cheng, T. Mura, L. M. Keer, Micromechanics modeling of crack initiation under contact fatigue, Journal of Tribology 116 (1) (1994) 2–8. doi:10.1115/1.2927042.
[184] A. Melander, A finite element study of short cracks with different inclusion types under rolling contact fatigue load, International Journal of Fatigue 19 (1) (1997) 13–24. doi:10.1016/S0142-1123(96)00045-X.
[185] A. Vincent, G. Lormand, P. Lamagnere, L. Gosset, D. Girodin, G. Dudragne, R. Fougeres, From white etching areas formed around inclusions to crack nucleation in bearing steels under rolling contacts, in: J. J. C. Hoo, W. B. Green (Eds.), Bearing Steels: Into the 21st century, no. ASTM STP 1327, American Society of Testing and Materials, West Conshohocken, PA 19428-2959, 1998, pp. 109–123.
[186] T. A. Harris, W. K. Yu, Lundberg–Palmgren fatigue theory: considerations of failure stress and stressed volume, Journal of Tribology 121 (1) (1999) 85–89. doi:10.1115/1.2833815.
[187] J. W. Ringsberg, Life prediction of rolling contact fatigue crack initiation, International Journal of Fatigue 23 (7) (2001) 575–586. doi:10.1016/S0142-1123(01)00024-X.
[188] N. Raje, F. Sadeghi, R. G. Rateick, A statistical damage mechanics model for subsurface initiated spalling in rolling contacts, Journal of Tribology 130 (4) (2008) 042201 (11 pages). doi:10.1115/1.2959109.
[189] N. Raje, F. Sadeghi, R. G. Rateick, M. R. Hoeprich, A numerical model for life scatter in rolling element bearings,

Journal of Tribology 130 (1) (2007) 011011 (10 pages). doi:10.1115/1.2806163.
[190] N. Raje, F. Sadeghi, Statistical numerical modelling of sub-surface initiated spalling in bearing contacts, Proceedings of the Institution of Mechanical Engineers, Part J: Journal of Engineering Tribology 223 (6) (2009) 849–858. doi:10.1243/13506501JET481.
[191] T. S. Slack, F. Sadeghi, Explicit finite element modeling of subsurface initiated spalling in rolling contacts, Tribology International 43 (9) (2010) 1693–1702. doi:10.1016/j.triboint.2010.03.019.
[192] W. Weibull, A statistical theory of strength of materials, Ingeniörsvetenskapsakademien handlingar, Proceedings of the Royal Swedish Institute for Engineering and Research (151).
[193] W. Weibull, A statistical representation of fatigue failure in solids, Acta Politechnica Mechanical Engineering Series 1 (9, 49), Royal Swedish Academy of Engineering Sciences.
[194] T. E. Tallian, Weibull distribution of rolling contact fatigue life and deviations therefrom, Transactions of the American Society of Lubrication Engineers 5 (1) (1962) 183–196. doi:10.1080/05698196208972465.
[195] D. Dowson, G. R. Higginson, A numerical solution to the elasto-hydrodynamic problem, Journal of Mechanical Engineering Science 1 (1) (1959) 6–15. doi:10.1243/JMES_JOUR_1959_001_004_02.
[196] D. Dowson, G. R. Higginson, Elasto-hydrodynamic lubrication: the fundamentals of roller and gear lubrication, Pergamon Press, 1966.
[197] B. J. Hamrock, W. J. Anderson, Rolling element bearings, Tech. Rep. NASA RP-1105, National Aeronautics and Space Administration, Lewis Research Center, Cleveland, Ohio 44135-3191 (June 1983).
[198] D. Dowson, Elastohydrodynamic and micro-elastohydrodynamic lubrication, Wear 190 (2) (1995) 125–138. doi:10.1016/0043-1648(95)06660-8.
[199] D. Dowson, History of Tribology, Second Edition, Longman, New York, 1999.
[200] Y. H. Wijnant, J. A. Wensing, G. C. Nijen, The influence of lubrication on the dynamic behaviour of ball bearings, Journal of Sound and Vibration 222 (4) (1999) 579–596. doi:10.1006/jsvi.1998.2068.
[201] H. A. Spikes, A. V. Olver, Basics of mixed lubrication, Lubrication Science 16 (1) (2003) 3–28. doi:10.1002/ls.3010160102.
[202] American National Standard (ANSI / AFBMA) Standard 9-1990 — Load rating and fatigue life for ball bearings.
[203] American National Standard (ANSI / AFBMA) Standard 11-1990 — Load rating and fatigue life for roller bearings.
[204] E. V. Zaretsky, A. Palmgren revisited — a basis for bearing life prediction, Tech. Rep. E-10555, National Aeronautics and Space Administration, Lewis Research Center, Cleveland, Ohio 44135-3191 (April 1997).
[205] R. Stribeck, Ball bearings for various loads, Transactions of the American Society of Mechanical Engineers 29 (1907) 420–463.
[206] H. Sjoväll, The load distribution within ball and roller bearings under given external radial and axial load, Teknisk Tidskrift, Mekanik 9 (1933) 97–102.
[207] A. B. Jones, Analysis of stresses and deflections, New Departure Division, General Motors Corporation, 1946.
[208] A. B. Jones, A general theory for elastically constrained ball and radial roller bearings under arbitrary load and speed conditions, Journal of Fluids Engineering 82 (2) (1960) 309–320. doi:10.1115/1.3662587.
[209] M. J. Lighthill, An Introduction to Fourier Analysis and Generalised Functions, Cambridge University Press, 1958.
[210] R. N. Bracewell, The Fourier Transform and Its Applications, Third Edition, McGraw-Hill Education, 2000.
[211] M. S. Darlow, R. H. Badgley, G. W. Hogg, Application of high frequency resonance techniques for bearing diagnostics in helicopter gearboxes, Tech. rep., US Army Air Mobility Research and Development Laboratory (1974).
[212] P. D. McFadden, J. D. Smith, The vibration monitoring of rolling element bearings by the high-frequency resonance technique — a review, Tribology International 17 (1) (1984) 3–10. doi:10.1016/0301-679X(84)90076-8.
[213] D. Ho, Bearing diagnostics and self-adaptive noise cancellation, Ph.D. thesis, School of Mechanical and Manufacturing Engineering, The University of New South Wales, Sydney NSW 2052, Australia (1999).
[214] W. Gardner, Cyclostationarity in communications and signal processing, IEEE Press, 1994.
[215] A. C. McCormick, A. K. Nandi, Cyclostationarity in rotating machine vibrations, Mechanical Systems and Signal Processing 12 (2) (1998) 225–242. doi:10.1006/mssp.1997.0148.
[216] J. Antoni, Cyclic spectral analysis in practice, Mechanical Systems and Signal Processing 21 (2) (2007) 597–630. doi:10.1016/j.ymssp.2006.08.007.
[217] J. Antoni, Cyclic spectral analysis of rolling-element bearing signals: Facts and fictions, Journal of Sound and Vibration 304 (3–5) (2007) 497–529. doi:10.1016/j.jsv.2007.02.029.
[218] J. Antoni, Cyclostationarity by examples, Mechanical Systems and Signal Processing 23 (4) (2009) 987–1036. doi:10.1016/j.ymssp.2008.10.010.
[219] J. A. Greenwood, J. B. P. Williamson, Contact of nominally flat surfaces, Proceedings of the Royal Society of London. Series A, Mathematical, Physical and Engineering Sciences 295 (1442) (1966) 300–319. doi:10.1098/rspa.1966.0242.
[220] J. A. Greenwood, J. H. Tripp, The elastic contact of rough spheres, Journal of Applied Mechanics 34 (1) (1967) 153–159. doi:10.1115/1.3607616.
[221] J. A. Greenwood, The area of contact between rough surfaces and flat, Journal of Lubrication Technology 89 (1) (1967) 81–87. doi:10.1115/1.3616906.
[222] C. C. Lo, Elastic contact of rough cylinders, International Journal of Mechanical Science 11 (1) (1969) 105–115. doi:10.1016/0020-7403(69)90083-6.
[223] J. A. Greenwood, J. H. Tripp, The contact of two nominally flat rough surfaces, Proceedings of the Institution of Mechanical Engineers 185 (1) (1970) 625–633. doi:10.1243/PIME_PROC_1970_185_069_02.
[224] K. L. Johnson, J. A. Greenwood, S. Y. Poon, A simple theory of asperity contact in elastohydrodynamic lubrication, Wear 19 (1) (1972) 91–108. doi:10.1016/0043-1648(72)90445-0.

[225] R. A. Onions, J. F. Archard, The contact of surfaces having a random structure, Journal of Physics D: Applied Physics 6 (3) (1973) 289–304. doi:10.1088/0022-3727/6/3/302.
[226] A. W. Bush, R. D. Gibson, The elastic contact of a rough surface, Wear 35 (1) (1975) 87–111. doi:10.1016/0043-1648(75)90145-3.
[227] J. I. McCool, Comparison of models for the contact of rough surfaces, Wear 107 (1) (1986) 37–60. doi:10.1016/0043-1648(86)90045-1.
[228] J. I. McCool, Relating profile instrument measurement to the function performance of rough surfaces, Journal of Tribology 109 (2) (1987) 264–270. doi:10.1115/1.3261349.
[229] P. J. Remington, Wheel/rail noise — Part I: Characterization of the wheel/rail dynamic system, Journal of Sound and Vibration 46 (3) (1976) 359–379. doi:10.1016/0022-460X(76)90861-0.
[230] P. J. Remington, Wheel/rail noise — Part IV: Rolling noise, Journal of Sound and Vibration 46 (3) (1976) 419–436. doi:10.1016/0022-460X(76)90864-6.
[231] P. J. Remington, Wheel/rail rolling noise: What do we know? what don't we know? where do we go from here?, Journal of Sound and Vibration 120 (2) (1988) 203–226. doi:10.1016/0022-460X(88)90430-0.
[232] M. L. Munjal, M. Heckl, Some mechanisms of excitation of a railway wheel, Journal of Sound and Vibration 81 (4) (1982) 477–489. doi:10.1016/0022-460X(82)90291-7.
[233] D. J. Thompson, Wheel–rail noise generation, Part I: Introduction and interaction model, Journal of Sound and Vibration 161 (3) (1993) 383–400. doi:10.1006/jsvi.1993.1082.
[234] D. J. Thompson, Wheel–rail noise generation, Part II: Wheel vibration, Journal of Sound and Vibration 161 (3) (1993) 401–419. doi:10.1006/jsvi.1993.1083.
[235] D. J. Thompson, Wheel–rail noise generation, Part III: Rail vibration, Journal of Sound and Vibration 161 (3) (1993) 421–446. doi:10.1006/jsvi.1993.1084.
[236] D. J. Thompson, Wheel–rail noise generation, Part IV: Contact zone and results, Journal of Sound and Vibration 161 (3) (1993) 447–466. doi:10.1006/jsvi.1993.1085.
[237] D. J. Thompson, Wheel–rail noise generation, Part V: Inclusion of wheel rotation, Journal of Sound and Vibration 161 (3) (1993) 467–482. doi:10.1006/jsvi.1993.1086.
[238] D. J. Thompson, On the relationship between wheel and rail surface roughness and rolling noise, Journal of Sound and Vibration 193 (1) (1996) 149–160. doi:10.1006/jsvi.1996.0254.
[239] D. Thompson, Railway Noise and Vibration, First Edition, Elsevier, 2009.
[240] R. S. Sayles, S. Y. Poon, Surface topography and rolling element vibration, Journal of Precision Engineering 3 (3) (1981) 137–144. doi:10.1016/0141-6359(81)90004-0.
[241] S. Y. Poon, F. P. Wardle, Rolling bearing noise — cause and cure (July/August 1983).
[242] J. S. Bendat, A. G. Piersol, Random Data: Analysis and Measurement Procedures, Fourth Edition, Wiley Series in Probability and Statistics, Wiley, 2010.
[243] SKF, Svenska Kullagerfabriken AB, Gothenburg, Sweden.
URL http://www.skf.com/
[244] A. Liew, N. S. Feng, E. J. Hahn, Transient rotordynamic modeling of rolling element bearing systems, Journal of Engineering for Gas Turbines and Power 124 (4) (2002) 984–991. doi:10.1115/1.1479337.
[245] J. D. Lambert, Numerical Methods for Ordinary Differential Systems: The Initial Value Problem, John Wiley & Sons, 2000.
[246] M. F. While, Vibration transmission characteristics of bearings related to machinery condition monitoring, Tech. Rep. 96, Institute of Sound and Vibration Research, University of Southampton, UK (1977).
[247] M. F. While, Rolling element bearing vibration transfer characteristics: Effect of stiffness, Journal of Applied Mechanics 46 (3) (1979) 677–684. doi:10.1115/1.3424626.
[248] C. Zhang, T. R. Kurfess, S. Danyluk, S. Y. Liang, Impact dynamics modelling of bearing vibration for defect size estimation, International Journal of COMADEM 3 (3) (2000) 37–42.
[249] Simulink®, The MathWorks, Inc.
URL http://www.mathworks.com
[250] MATLAB®, The MathWorks, Inc.
URL http://www.mathworks.com
[251] Bearing Data Centre, Case Western Reserve University, (accessed 13 September 2014).
URL http://csegroups.case.edu/bearingdatacenter/pages/download-data-file
[252] P. Raveendranath, G. Singh, B. Pradhan, A two-noded locking-free shear flexible curved beam element, International Journal for Numerical Methods in Engineering 44 (2) (1999) 265–280. doi:10.1002/(SICI)1097-0207(19990120)44:2<265::AID-NME505>3.0.CO;2-K.
[253] Adams, Release 2008 r1, MSC Software Corporation.
URL http://www.mscsoftware.com/product/adams
[254] H. M. Paynter, Analysis and design of engineering systems, M.I.T. Press, Boston, 1961.
[255] RecurDyn™, Release V8R1, FunctionBay, Inc.
URL http://eng.functionbay.co.kr/
[256] J. C. Houbolt, A recurrence matrix solution for the dynamic response of elastic aircraft, Journal of the Aeronautical Sciences 17 (9) (1950) 540–550.
[257] N. M. Newmark, A method of computation for structural dynamics, Journal of the Engineering Mechanics Division 85 (3) (1959) 67–94.
[258] E. L. Wilson, I. Farhoomand, K. J. Bathe, Nonlinear dynamic analysis of complex structures, Earthquake Engineering

and Structural Dynamics 1 (3) (1973) 241–252. doi:10.1002/eqe.4290010305.
[259] I. Gladwell, R. Thomas, Stability properties of the Newmark, Houbolt and Wilson Theta methods, International Journal for Numerical and Analytical Methods in Geomechanics 4 (2) (1980) 143–158. doi:10.1016/0148-9062(81)90280-1.
[260] K. Subbaraj, M. A. Dokainish, A survey of direct time-integration methods in computational structural dynamics — II. Implicit methods, Computer and Structures 32 (6) (1989) 1387–1401. doi:10.1016/0045-7949(89)90315-5.
[261] W. L. Wood, Practical time-stepping schemes, Oxford applied mathematics and computing science series, Oxford: Clarendon Press, 1990.
[262] K. J. Bathe, Finite element procedures, Prentice Hall, 1996.
[263] K. J. Bathe, G. Noh, Insight into an implicit time integration scheme for structural dynamics, Computer and Structures 98–99 (2012) 1–6. doi:10.1016/j.compstruc.2012.01.009.
[264] C. Runge, Über die numerische auflösing von differentialgleichungen, Mathematische Annalen 46 (1985) 167–178.
[265] M. W. Kutta, Beitrag zur näherungsweisen integration totaler differentialgleichungen, Zeitschrift für angewandte Mathematik und Physik 46 (1901) 435–453.
[266] G. Dahlquist, A special stability problem for linear multistep methods, BIT Numerical Mathematics 3 (1) (1963) 27–43. doi:10.1007/BF01963532.
[267] M. Abramowitz, Handbook of Mathematical Functions: with Formulas, Graphs, and Mathematical Tables, Ninth Edition, Dover Books on Mathematics, Dover Publications, New York, 1972.
[268] R. D. Krieg, Unconditional stability in numerical time integration methods, Journal of Applied Mechanics 40 (2) (1973) 417–421. doi:10.1115/1.3422999.
[269] P. S. Jensen, Transient analysis of structures by stiffly stable methods, Computer and Structures 4 (3) (1974) 615–626. doi:10.1016/0045-7949(74)90010-8.
[270] J. L. Humar, E. W. Wright, Numerical methods in structural dynamics, Canadian Journal of Civil Engineering 1 (2) (1974) 179–193. doi:10.1139/l74-017.
[271] M. A. Dokainish, K. Subbaraj, A survey of direct time-integration methods in computational structural dynamics — I. Explicit methods, Computer and Structures 32 (6) (1989) 1371–1386. doi:10.1016/0045-7949(89)90314-3.
[272] J. Chung, J. M. Lee, A new family of explicit time integration methods for linear and non-linear structural dynamics, International Journal for Numerical Methods in Engineering 37 (23) (1994) 3961–3976. doi:10.1002/nme.1620372303.
[273] G. M. Hulbert, J. Chung, Explicit time integration algorithms for structural dynamics with optimal numerical dissipation, Computer Methods in Applied Mechanics and Engineering 137 (2) (1996) 175–178. doi:10.1016/S0045-7825(96)01036-5.
[274] G. Noh, K. J. Bathe, An explicit time integration scheme for the analysis of wave propagations, Computer and Structures 129 (2013) 178–193. doi:10.1016/j.compstruc.2013.06.007.
[275] I-DEAS, Siemens PLM Software.
URL http://www.plm.automation.siemens.com/en_us/products/nx/ideas/
[276] ANSYS, Release 14.5, ANSYS Inc.
URL http://www.ansys.com/
[277] Abaqus, Release 6.13, Dassault Systèmes.
URL http://www.3ds.com/products-services/simulia/portfolio/abaqus/overview/
[278] ADINA — Automatic Dynamic Incremental Nonlinear Analysis, Release 9.0.0, ADINA R & D, Inc.
URL http://www.adina.com/index.shtml
[279] Simulation Mechanical, Autodesk Inc., formerly known as ALGOR Simulation.
URL http://www.autodesk.com/products/autodesk-simulation-family/features/simulation-mechanical/all/gallery-view
[280] MSC Nastran, MSC Software Corporation.
URL http://www.mscsoftware.com/product/msc-nastran
[281] M. R. Lovell, M. M. Khonsari, R. D. Marangoni, A finite element analysis of the frictional forces between a cylindrical bearing element and MoS2, coated and uncoated surfaces, Wear 194 (1–2) (1996) 60–70. doi:10.1016/0043-1648(95)06708-6.
[282] M. R. Lovell, M. M. Khonsari, R. D. Marangoni, Frictional analysis of MoS2 coated ball bearings: A three-dimensional finite element analysis, Journal of Tribology 119 (4) (1997) 754–763. doi:10.1115/1.2833881.
[283] F. M. A. El-Saeidy, Finite element modeling of a rotor shaft rolling bearings system with consideration of bearing nonlinearities, Journal of Vibration and Control 4 (4) (1998) 541–602. doi:10.1177/107754639800400503.
[284] A. Bourdon, J. F. Rigal, D. Play, Static rolling bearing models in a C.A.D. environment for the study of complex mechanisms: Part I — Rolling bearing model, Journal of Tribology 121 (2) (1999) 205–214. doi:10.1115/1.2833923.
[285] A. Bourdon, J. F. Rigal, D. Play, Static rolling bearing models in a C.A.D. environment for the study of complex mechanisms: Part II — Complete assembly model, Journal of Tribology 121 (2) (1999) 215–223. doi:10.1115/1.2833924.
[286] A. Malhi, Finite element modeling of vibrations caused by a defect in the outer ring of a ball bearing, Tech. rep., University of Massachusetts (2002).
[287] R. Kunc, I. Prebil, Numerical determination of carrying capacity of large rolling bearings, Journal of Materials Processing Technology 155–156 (30) (2004) 1696–1703. doi:10.1016/j.jmatprotec.2004.04.125.
[288] L. Kania, Modelling of rollers in calculation of slewing bearing with the use of finite elements, Mechanism and Machine Theory 41 (11) (2006) 1359–1376. doi:10.1016/j.mechmachtheory.2005.12.007.
[289] H. Rubio, J. C. Prada, C. Castejón, E. Laniado, Dynamic analysis of rolling bearing system using Lagrangian model vs FEM code, in: 12^{th} IFToMM World Congress, Besancon, France, 2007.
[290] N. Demirhan, B. Kanber, Stress and displacement distributions on cylindrical roller bearing rings using FEM, Mechanics Based Design of Structures and Machines: An International Journal 36 (1) (2008) 86–102. doi:10.1080/15397730701842537.

[291] A. Daidié, Z. Chaib, A. Ghosn, 3D simplified finite elements analysis of load and contact angle in a slewing ball bearing, Journal of Mechanical Design 130 (8) (2008) 082601 (8 pages). doi:10.1115/1.2918915.
[292] N. A. Branch, N. K. Akakere, V. Svendsen, N. H. Forster, Stress field evolution in a ball bearing raceway fatigue spall, Journal of ASTM International 7 (2) (2010) 1–18. doi:10.1520/JAI102529.
[293] Y. Guo, R. G. Parker, Stiffness matrix calculation of rolling element bearings using a finite element/contact mechanics model, Mechanism and Machine Theory 51 (2012) 32–45. doi:10.1016/j.mechmachtheory.2011.12.006.
[294] J. Aguirrebeitia, M. Abasolo, R. Avilés, I. F. de Bustos, General static load-carrying capacity for the design and selection of four contact point slewing bearings: Finite element calculations and theoretical model validation, Finite Elements in Analysis and Design 55 (2012) 23–30. doi:10.1016/j.finel.2012.02.002.
[295] E. Laniado-Jácoe, J. Meneses-Alonso, V. Diaz-López, A study of sliding between rollers and races in a roller bearing with a numerical model for mechanical event simulations, Tribology International 43 (11) (2010) 2175–2182. doi:10.1016/j.triboint.2010.06.014.
[296] S. Deng, L. Hua, X. Han, S. Huang, Finite element analysis of fatigue life for deep groove ball bearing, Proceedings of the Institution of Mechanical Engineers, Part L: Journal of Materials Design and Applications 227 (1) (2013) 70–81. doi:10.1177/1464420712445968.
[297] P. Göncz, M. Drobne, S. Glodež, Computational model for determination of dynamic load capacity of large three-row roller slewing bearings, Engineering Failure Analysis 32 (2013) 44–53. doi:10.1016/j.engfailanal.2013.02.030.
[298] J. O. Hallquist, LS-DYNA Theory Manual, Livermore Software Technology Corporation (March 2006).
[299] ANSYS Autodyn, Release 14.5, ANSYS IP, Inc.
URL http://www.ansys.com/Products/Simulation+Technology/Structural+Analysis/Explicit+Dynamics/ANSYS+Autodyn
[300] L. Fan, N.-L. Tan, D.-P. Shen, FEA on stress field of rolling element bearing based on explicit dynamics, Journal of Beijing Jiaotong University 4 (2006) 109–112.
[301] Q. Rong, T. Lin, Y. Shao, Finite element simulation of the motion process for deep-groove ball bearing, Journal of Advanced Manufacturing Systems 7 (1) (2008) 9–13. doi:10.1142/S0219686708001024.
[302] T.-J. Lin, Q. Rong, L. Runfang, Y.-M. Shao, Finite element analysis for dynamic characteristic of a deep-groove ball bearing in motion process, Journal of Vibration and Shock 28 (1) (2009) 118–122.
[303] Y. Zhang, Y. Xie, X. Wu, W. Lu, Finite element analysis for dynamic characteristic of deep-groove ball bearing operating from acceleration to constant speed, Journal of Northeastern University 33 (1) (2012) 103–107.
[304] Livermore Software Technology Corporation, Livermore, California 94551-0712, LS-DYNA Keyword User's Manual, Volume I (February 2012).
[305] ANSYS, Release 14.5, Help System, Structural Anslysis Guide, ANSYS, Inc.
[306] M. R. Hoeprich, Rolling element bearing fatigue damage progression, Journal of Tribology 114 (2) (1992) 328–333. doi:10.1115/1.2920891.
[307] P. A. Boto, Detection of bearing damage by shock pulse measurement, Ball Bearing Journal 167 (1971) 1–7.
[308] S. Gade, K. G. Hansen, Non-stationary signal analysis using wavelet transform, short-time Fourier transform and Wigner-Ville distribution, Technical Review 2, Brüel & Kjær (1996).
[309] P. W. Tse, Y. H. Peng, R. Yam, Wavelet analysis and envelope detection for rolling element bearing fault diagnosis — their effectiveness and flexibilities, Transactions of the American Society of Lubrication Engineers, Journal of Vibration and Acoustics 123 (2001) 303–310. doi:10.1115/1.1379745.
[310] E. Wigner, On the quantam corrections for thermodynamic equilibrium, Physical Review 40 (5) (1932) 749–759. doi:10.1103/PhysRev.40.749.
[311] J. Ville, Theory et application de la notion de signal analytique, Cables et Transmissions 20A.
[312] N. Baydar, A. Ball, A comparative study of acoustic and vibration signals in detection of gear failures using Wigner-Ville distribution, Mechanical Systems and Signal Processing 15 (6) (2001) 1091–1107. doi:10.1006/mssp.2000.1338.
[313] D. C. Baillie, J. Mathew, A comparison of autoregressive modeling techniques for fault diagnosis of rolling element bearings, Mechanical Systems and Signal Processing 10 (1) (1996) 1–17. doi:10.1006/mssp.1996.0001.
[314] C. Junsheng, Y. Dejie, Y. Yu, A fault diagnosis approach for roller bearings based on EMD method and AR model, Mechanical Systems and Signal Processing 20 (2) (2006) 350–362. doi:10.1016/j.ymssp.2004.11.002.
[315] J. Morlet, G. Arens, E. Fourgeau, D. Giard, Wave propagation and sampling theory — Part II: Sampling theory and complex waves, Geophysics 47 (2) (1982) 222–236. doi:10.1190/1.1441329.
[316] J. Lin, L. Qu, Feature extraction based on Morlet wavelet and its application for mechanical fault diagnosis, Journal of Sound and Vibration 234 (1) (2000) 135–148. doi:10.1006/jsvi.2000.2864.
[317] N. Thrane, Hilbert transform, Technical Review 3, Brüel and Kjær (1984).
[318] M. Feldman, Hilbert transform in vibration analysis, Mechanical Systems and Signal Processing 25 (3) (2011) 735–802. doi:10.1016/j.ymssp.2010.07.018.
[319] B. P. Bogert, M. J. R. Healy, J. W. Tuckey, The quefrequency analysis of time series for echoes: cepstrum, psuedo-autocovariance, cross-cepstrum and saphe cracking, in: M. Rosenblatt (Ed.), Proceedings of Symposium on Time Series Analysis, Wiley, N.Y., 1963, pp. 209–243.
[320] D. G. Childers, D. P. Skinner, R. C. Kemerait, The cepstrum: A guide to processing, Proceedings of IEEE 65 (10) (1977) 1428–1443. doi:10.1109/PROC.1977.10747.
[321] R. B. Randall, J. Hee, Cepstrum analsysis, Technical Review 3, Brüel and Kjær (1981).
[322] S. M. Pincus, Approximate entropy as a complexity measure, Chaos 5 (1) (1995) 110–117. doi:10.1063/1.166092.
[323] Y. Yu, Y. Dejie, C. Junsheng, A roller bearing fault diagnosis method based on EMD energy entropy and ANN, Journal of Sound and Vibration 294 (1–2) (2006) 269–277. doi:10.1016/j.jsv.2005.11.002.
[324] R. Yan, R. X. Gao, Approximate entropy as a diagnostic tool for machine health monitoring, Mechanical Systems and

Signal Processing 21 (2) (2007) 824–839. doi:10.1016/j.ymssp.2006.02.009.
[325] Y. He, X. Zhang, Approximate entropy analysis of the acoustic emission from defects in rolling element bearings, Journal of Vibration and Acoustics 134 (6) (2012) 061012 (8 pages). doi:10.1115/1.4007240.
[326] T. A. Harris, M. H. Mindel, Rolling element bearing dynamics, Wear 23 (3) (1973) 311–337. doi:10.1016/0043-1648(73)90020-3.
[327] P. K. Gupta, Transient ball motion and skid in ball bearings, Journal of Lubrication Technology 97 (2) (1975) 261–269. doi:10.1115/1.3452568.
[328] P. K. Gupta, Dynamics of rolling-element bearings — Part I: Cylindrical roller bearing analysis, Journal of Lubrication Technology 101 (3) (1979) 293–302. doi:10.1115/1.3453357.
[329] P. K. Gupta, Dynamics of rolling-element bearings — Part II: Cylindrical roller bearing results, Journal of Lubrication Technology 101 (3) (1979) 305–311. doi:10.1115/1.3453360.
[330] P. K. Gupta, Dynamics of rolling-element bearings — Part III: Ball bearing analysis, Journal of Lubrication Technology 101 (3) (1979) 312–318. doi:10.1115/1.3453363.
[331] P. K. Gupta, Dynamics of rolling-element bearings — Part IV: Ball bearing results, Journal of Lubrication Technology 101 (3) (1979) 319–326. doi:10.1115/1.3453364.
[332] F. P. Wardle, S. J. Lacey, S. Y. Poon, Dynamic and static characteristics of a wide speed range machine tool spindle, Precision Enginering 5 (4) (1983) 175–183. doi:10.1016/0141-6359(83)90097-1.
[333] P. K. Gupta, J. F. Dill, M. E. Bandow, Dynamics of rolling element-bearings experimental validation of the DREB and RAPIDREB computer programs, Journal of Tribology 107 (1) (1985) 132–137. doi:10.1115/1.3260989.
[334] P. K. Gupta, T. E. Tallian, Rolling bearing life prediction-correction for materials and operating conditions — Part III: Implementation in bearing dynamics computer codes, Journal of Tribology 112 (1) (1990) 23–26. doi:10.1115/1.2920226.
[335] T. C. Lim, R. Singh, Vibration transmission through rolling element bearings, Part I: Bearing stiffness formulation, Journal of Sound and Vibration 139 (2) (1990) 179–199. doi:10.1016/0022-460X(90)90882-Z.
[336] T. C. Lim, R. Singh, Vibration transmission through rolling element bearings, Part II: System studies, Journal of Sound and Vibration 139 (2) (1990) 201–225. doi:10.1016/0022-460X(90)90883-2.
[337] T. C. Lim, R. Singh, Vibration transmission through rolling element bearings, Part III: Geared rotor system studies, Journal of Sound and Vibration 151 (1) (1991) 31–54. doi:10.1016/0022-460X(91)90650-9.
[338] T. C. Lim, R. Singh, Vibration transmission through rolling element bearings, Part IV: Statistical energy analysis, Journal of Sound and Vibration 153 (1) (1992) 37–50. doi:10.1016/0022-460X(92)90625-8.
[339] T. C. Lim, R. Singh, Vibration transmission through rolling element bearings, Part V: Effect of distributed contact load on roller bearing stiffness matrix, Journal of Sound and Vibration 169 (4) (1994) 547–553. doi:10.1006/jsvi.1994.1033.
[340] T. A. Harris, R. M. Barnsby, Life ratings for ball and roller bearings, Proceedings of the Institution of Mechanical Engineers, Part J: Journal of Engineering Tribology 215 (6) (2001) 577–595. doi:10.1243/1350650011543817.
[341] A. Gunduz, R. Singh, Stiffness matrix formulation for double row angular contact ball bearings: Analytical development and validation, Journal of Sound and Vibration 332 (22) (2013) 5898–5916. doi:10.1016/j.jsv.2013.04.049.
[342] ADORE — Advanced Dynamics of Rolling Elements, Release 5.7, PKG Inc.
URL http://www.pradeepkguptainc.com/Adore.html
[343] COBRA ™—Computer Optimized Ball and Roller bearing Analysis software, J.V. Poplawski & Associates.
URL http://www.bearingspecialists.com/software.asp
[344] L.-E. Stacke, D. Fritzson, P. Nordling, BEAST — a rolling bearing simulation tool, Proceedings of the Institution of Mechanical Engineers, Part K: Journal of Multi-body Dynamics 213 (2) (1999) 63–71. doi:10.1243/1464419991544063.
[345] M. Sekiya, Integrated Bearing Dynamic Analysis System (IBDAS), Technical Review 79, NTN Corporation, Osaka, Japan (2011).
[346] RailBAM ® — Railway Bearing Acoustic Monitor, (accessed 13 September 2014).
URL http://www.trackiq.com.au/railbam.html
[347] J. E. Bambara, J. L. Frarey, R. L. Smith, On-line acoustic detection of bearing defects, United States Patent 4790190 (December 1988).
[348] J. E. Bambara, Acoustic detection of bearing defects, United States Patent 4843885 (July 1989).
[349] J. E. Bambara, Integrity test for acoustic bearing defect detector, United States Patent 5029477 (July 1991).
[350] J. E. Bambara, Acoustic bearing defect detector, United States Patent 5150618 (September 1992).
[351] K. Bladon, D. Rennison, G. Izbinsky, R. Tracy, T. Baldon, Predictive condition monitoring of railway rolling stock, in: Proceedings of Conference on Railway Engineering CORE 2004: New Horizons for Rail, Railway Technical Society of Australasia, Darwin, N.T., Australia, 2004, pp. 22.1–22.12.
[352] C. Southern, D. Rennison, U. Köpke, RailBAM® — An advanced bearing acoustic monitor: Initial operational performance results, in: Proceedings of Conference on Railway Engineering CORE 2004: New Horizons for Rail, Railway Technical Society of Australasia, Darwin, N.T., Australia, 2004, pp. 23.01–23.07.
[353] U. Köpke, P. Lindqvist, A. Meyer, D. Rennison, Development and verification of an advanced bearing acoustic monitor, in: Proceedings of the TTCI Bearing Symposium, Chicago, USA, 2007.
[354] C. Southern, M. Sowden, R. Donnelly, Maintenance planning using BAM's, in: Proceedings of the TTCI Bearing Symposium, Chicago, USA, 2007.